SAPIENZA
Università di Roma
Facoltà di Scienze Matematiche Fisiche e Naturali

DOTTORATO DI RICERCA
IN GENETICA E BIOLOGIA MOLECOLARE

XXXII Ciclo
(A.A. 2018/2019)

Analysis of role of AKTIP at different stages of cell division

Dottorando
Simona del Giudice

Docente guida
Prof. Isabella Saggio

Tutore
Prof. Fiammetta Vernì

Coordinatore
Prof. Fulvio Cruciani

INDEX

SUMMARY

AKTIP is a recently discovered non-shelterin telomeric protein, whose deficiency generates telomere fragility by impinging on replication (Burla et al., 2015). As previusly described, AKTIP interacts with lamins and its downregulation triggers a premature aging phenotype both at cellular level and at organismal level (in a mouse model knocked down for its murine homologue Ft1) recalling those of progeroid patients with mutations in LMNA gene (Burla et al., 2016; La Torre et. al., 2018). Another AKTIP peculiarity is its intracellular distribution: in interphases cells AKTIP is located, as discrete foci, both in the cytoplasm and in the nucleus, where it is especially enriched at nuclear envelope. In mitosis AKTIP is located at spindle matrix in metaphase and then it is enriched in anaphase at the bridge structure connecting the two newly formed cells, called midbody (Burla et al., 2015; 2016).

Given these premises, this work aims at thouroughly investigating the AKTIP role and distribution at these two important cellular compartments.

Concerning AKTIP at nuclear periphery we focused our attention on its relationship with lamins both in physiological and pathological conditions. The nuclear lamina is a structure positioned between the nuclear envelope and the chromatin and has been involved in different processes: the nuclear architecture and DNA metabolism. Mutations in the lamin A encoding gene result in a wide range of rare diseases named laminopathies. The most widely studied, among them, is the Hutchinson-Gilford progeria syndrome (HGPS) (Butin-Israeli et al., 2012).

Using Structure Illumination Microscopy (SIM) (Schermelleh et al., 2010) we demonstrated that AKTIP is localized at nuclear rim in a close proximity with A-type lamins and that it is mislocated in cells from LMNA-mutations associated progeroid patients suggesting that this mislocalization at nuclear rim could contribute to the HGPS phenotype.

For AKTIP at midbody we described by SIM that AKTIP forms a super-molecular structure, with a shape of a ring, around microtubules at the center of the intercellular bridge where the

endosomal sorting complex required for transport (ESCRT) complex is recruited and acts to finalize abscission (Elia et al., 2011; Karasmanis et al., 2019). ESCRTs are protein complexes involved in membrane remodeling acting through their highly regulated sequential recruitment at target membrane in collaboration with associated proteins. ESCRTs participate in very different cellular processes requiring membrane remodeling including vesicles trafficking, abscission, nuclear envelope reformation and repair (Gatta and Carlton, 2019).

We also showed that AKTIP ring is in spatial proximity with ESCRT-III subunits, and functionally, AKTIP reduction impinges on ESCRT-III IST1 recruitment at the midbody and causes abscission defects, including longer abscission time and multinucleation.

The collected data and AKTIP intracellular distribution suggest that AKTIP could act as an ESCRT protein. This hypothesis is further supported by the structural and bioinformatics similarity with TSG101 and by the identification of putative partners

belonging to different ESCRTs involving pathways through a proteins interactions screening. We found that AKTIP interactes with an ESCRT-I member, the VPS28 subunit. Since VPS28 bridges the ESCRT-I to the ESCRT-II complex (Carlton and Martin-Serrano; 2007), these data make hypothesize a sequential pathway in which AKTIP is connected to ESCRT-II and then to ESCRT-III via VPS28.

In summary, these data taken together indicate AKTIP as a new candidate factor associated with the ESCRT complex functioning at nuclear envelope and in cytokinesis.

INTRODUCTION

The midbody is a transient structure that connects two daughter cells at the end of cytokinesis and localizes the site of abscission

Cell division is one of the most fundamental biological processes and is necessary for growth, development and reproduction in many organisms. During cytokinesis the two daughter cells remain connected for some time by an intracellular bridge structure known as midbody. The midbody is a transient structure which provides a platform for the recruitment and organization of many proteins that regulate the abscission, the physical separation of the two daughter cells (D'avino and Capalbo, 2016).

The midbody is composed by a bundle of microtubules, which contains at its centre an electron-dense area with a high concentration of proteins named ‘midbody matrix’. This matrix is flanked by regions that are usually referred as ‘midbody arms’. The midbody matrix corresponds to the central “bulge” of the midbody and this zone appears as a non-stained ‘dark region’ in

immunofluorescence images of cells stained for microtubules because the dense cluster of proteins that accumulate around microtubules prevents the access of anti-tubulin antibodies. Moreover, some of these proteins form a ring around the dark zone, which has led to the term ‘midbody ring’ (Figure 1) (D'avino and Capalbo, 2016).

This organelle originitates from the midzone, a bipolar microtuble array that assembles between sister chromatids during anaphase; conversion of midzone to midbody correlates positively with furrow ingression (Figure 1) (Hu et al., 2011). When furrow ingression is complete, two symmetric constrictions take shape on both sides of the midbody center, making the midbody look similar to a ‘bow tie’. Subsequently, the midbody becomes progressively thinner, an event most likely mediated by microtubule depolymerizing factors such as katanin and spastin (Connell et al., 2009; Matsuo et al., 2013), and ultimately an abscission site appears first at one side of the midbody. The midbody remnant is therefore typically inherited by one of the two daughter cells and

slowly eliminated by autophagy (Pohl et al., 2009). The main function of the midbody is presumably to localize abscission. The midbody breakage is driven by the ESCRT machinery and by the activity of microtubule-severing proteins (Gromley et al., 2005; Morita et al., 2007; Lee et al., 2008; Elia et al., 2011; Guizetti et al., 2011).

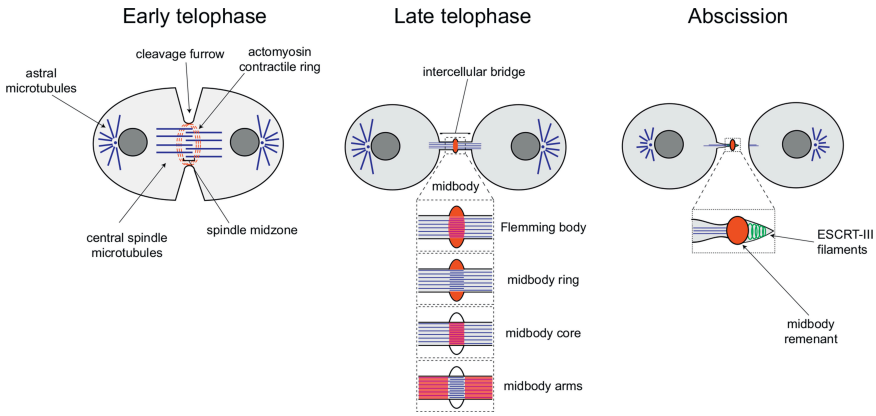

Figure 1: Schematic diagram illustrating the different stages of cytokinesis in animal cells. Microtubules are depicted in blue, the actomyosin contractile ring and various midbody regions in red (D'avino and Capalbo, 2016).

.

The endosomal sorting complex required for transport (ESCRT) is an evolutionarily conserved machinery for membrane scission processes

The ESCRT machinery is an ancient, evolutionarily preserved membrane remodelling complex that is deployed by cells to perform different physiological processes. The ESCRT proteins are key mediator of multivesicular body biogenesis (MVB), but they also play critical roles in retroviral budding, reformation of the nuclear envelope and cytokinetic abscission during mitotic exit (Figure 2) (Gatta and Caltron, 2019). The ESCRT machinery consists of biochemically distinct protein complexes named ESCRT-0, -I, -II, -III, and AAAATPase vacuolar protein-associated sorting 4 (VPS4), and the ALIX homodimer.

ESCRT-0 consists of two subunits, Hrs (hepatocyte growthfactor-regulated tyrosine kinase substrate) and STAM1/2 (signal transducing adaptor molecule1/2) (Vps27 and Hse1 in yeast), which functions as a 1:1 heterodimer (Asao et al., 1997; Bache et al., 2003; Ren et al., 2009). The ESCRT-0 complex is required for

MVB and binds to the clusters ubiquitinated cargo for delivery into MVB, recruiting clathrin, ubiquitin ligases, and deubiquitinating enzymes. In addition to this, Hrs contains a FYVE (Fab-1, YGL023, Vps27, and EEA1) zinc finger domain (Mao et al., 2000), which binds phosphatidylinositol 3-phosphate, PtdIns3P, and provides both membrane recruitment and endosomal specificity for the ESCRT-0 complex. The ESCRT-I machinery is recruited to sites of action by ESCRT-0 only in MVB, but different subfunction-specific targeting modules are involved in the other ESCRT mediated processes. These factors include CEP55 (cytokinesis) and Gag (virus budding), that are able to associate with ESCRT components and Bro1-domain proteins (Raiborg et al., 2001). ESCRT-I is an heteromeric complex composed by TSG101 (Vps23 in yeats), VPS28, VPS37, and hMVB12 (Bishop and Woodman, 2001; Katzmann et al., 2001; Bache et al., 2004; Chu et al., 2006; Curtiss et al., 2007). ESCRT-I interacts with ESCRT-0 on one end of the complex through the ubiquitin E2 variant domain (UEV), which corresponds to the N-terminus of

TSG101. The UEV binds to the PTAP-like motifs of the ESCRT-0 subunit VPS27/Hrs (Katzmann et al., 2003; Kostelansky et al., 2006). On the other end of the complex, ESCRT-I interacts with ESCRT-II and these two complexes appear to function as a 1:1 supercomplex (Gill et al., 2007). ESCRT-II is a Y-shaped heterotetramer composed by one subunit each of VPS22 (ELL-associated protein of 30 kDa, or EAP30) and VPS36 (EAP45), and two subunits of VPS25 (EAP20). ESCRT-II and ESCRT-III interact through the binding of VPS25. The high affinity bound between these two reveals their key role for ESCRT-II in initiating ESCRT-III complex formation (Babst et al., 2002; Langelier et al., 2006). Similarly to ESCRT-0 and -I, ESCRT-II binds ubiquitinated cargo, although only at one site (Alam et al., 2004). ESCRT-II appears to be nonessential for HIV-1 budding (Langelier et al., 2006) and cytokinesis (Morita et al., 2007), despite its central role in MVB biogenesis and membrane budding.

ESCRT-III proteins form a membrane-interacting oligomeric filament that is thought to operate the membrane remodelling

event, eventually resulting in scission (Hurley, 2015; Schoneberg et al., 2017; McCullough et al., 2018;).

ESCRT-III consists of four core subunits that in mammals are denoted as chargedmultivesicular body proteins (CHMPs) (CHMP6, CHMP4, CHMP3, CHMP2, and their isoforms) (Muziol et al., 2006; Bajorek et al., 2009). ESCRT-III monomers exist in an autoinhibited ‘‘closed’’ state in the cytoplasm, and they are activated when the ESCRT-II binding occurs (Teo et al., 2004). In addition to the ‘‘core’’ ESCRT-III subunits, there are several ‘‘accessory’’ ESCRT-III subunits, such as IST1, that govern ESCRT-III-Vps4 interactions. These modulate VPS4 function in three ways: by mediating VPS4 interactions with itself, with ESCRT-III subunits, and by promoting ATP hydrolysis (Azmi et al., 2006; Yu et al., 2008). VPS4 contains the main membrane remodeling and scission function of the ESCRT machinery (Gatta and Caltron, 2019).

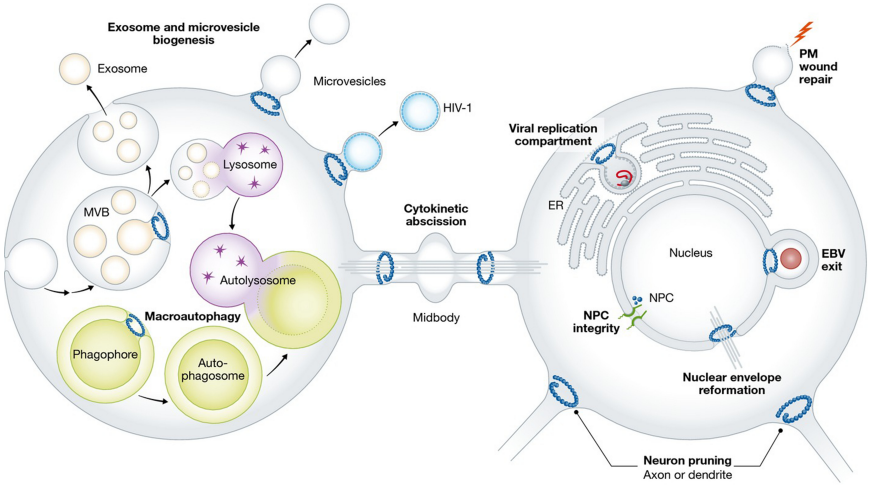

Figure 2: Overview of the cellular functions of the ESCRTs. ESCRT complexes catalyze a topologically distinct membrane-remodelling event: budding and scission of membranes away from the cytosol. During multivesicular body (MVB) sorting the ESCRT machinery generates intraluminal vesicles of MVBs to deliver ubiquitinated membrane proteins into lysosomes for degradation. During cytokinesis ESCRT complexes catalyze the final membrane abscission at the midbody. Additionally, the ESCRT machinery is required for the release of certain enveloped viruses (i.e. human immunodeficiency virus, HIV) from the surface of infected cells (Schmidt and Teis, 2012; Hurley 2015).

The ESCRT machinery is a kay mediator of abscission

Completion of cytokinesis requires abscission of the midbody, a membrane scission event that is topologically similar to MVB formation and it is know that the ESCRTs are critical mediators of this event (Carlton and Martin-Serrano, 2007; Morita et al., 2007; Carlton et al., 2008).

The current model for ESCRT function involves sequential membrane recruitment of different ESCRT components to orchestrate membrane scission. The event starts from the midbody component CEP55, which recruits the downstream partners needed for abscission. It is demostrated that cells show two alternative ways for assembling ESCRT-III at the midbody: one relies upon ALIX as an adaptor protein between CEP55 and ESCRT-III (Morita et al., 2007; Carlton et al., 2008) and the other involves a link via ESCRT-I, ESCRT-II and CHMP6 (Christ et al., 2016; Goliand et al., 2014) ESCRT-III assembly is highly dynamic and spatiotemporally ordered. It has been documented using 3D-STORM that initially ESCRT-III assembly into two rings adjacent

to the dark zone, subsequently ESCRT-III expands into helices and spirals that narrow down to the incipient site of abscission (Goliand et al., 2018). One important event in abscission is the recruitment of the ESCRT-III IST1. This protein is able to recruit during cytokinesis the ESCRT-III associated AAA-ATPase Spastin to the midbody to depolymerise microtubules and coordinate spindle disassembly with membrane sealing (Agromayor et al., 2009, Adell et al., 2011; Vietri et al., 2015).

More recently, it has been showed that ESCRTs also operate at the nuclear envelope during the mitotic exit. In this phase, they seal small holes in the reforming nuclear rim and coordinate this with removal of spindle-microtubules (Olmos et al., 2015; Vietri et al., 2015). ESCRT-III are recuited to the membrane by CHMP7; the N-terminus of CHMP7 acts as a novel membrane-binding module, that allows CHMP7 to bind to the ER and to provide a platform to direct NE recruitment of ESCRT-III through CHMP4B during mitotic exit (Olmos et al., 2016). Moreover, an essential role for ESCRT-III in controlling membrane integrity is emerging.

It is known that ESCRT-III can repair damaged regions of plasma membrane and so preserve cellular viability (Jimenez et al., 2014; Scheffer et al., 2014). Plasma membrane damage can be induced by interaction with the microenvironment or other external forces, for example nuclear deformation during cell migration leads to transient opening of the NE. It was demostrated that the ESCRT-III complex, similarly to what happens at mitotic exit, is required for fast resealing of the nucleo-cytoplasmic barrier. (Denais et al., 2016; Raab et al., 2016).

Nuclear lamins are one of major factor in the structural organization and function of the nucleus

In eukaryotic cells, chromatin is tightly packed in a highly organized manner within a nucleus that is composed of two main compartments: the nucleoplasm and the nuclear envelope (NE). The NE separates nuclear functions from cytoplasmic functions and at its inner surface it provides a docking site for chromatin. The major structural elements of the NE are the inner nuclear membrane (INM), the outer nuclear membrane (ONM), the nuclear pore complexes (NPCs), and the nuclear lamina. The lamina is comprised of a meshwork of proteins closely associated with the INM and attached to chromatin (Fawcett, 1966; Patrizi and Poger, 1967; Aaronson and Blobel, 1975). The main constituents of the lamina are the type V intermediate filament (IF) proteins named lamins. There are two types of lamins: A and B types. For A-type lamins exist two major isoforms, lamins A and C, that are derived from a single gene (LMNA) by alternative splicing (Lin and Worman, 1993). Lamins B1 and B2 are the two major B-type

lamins and are encoded by the LMNB1 and LMNB2 genes, respectively (Vorburger et al., 1989). The nuclear lamins show the characteristic tripartite structure of intermediate filament (IF) proteins: a long central α-helical rod domain, flanked by globular N-terminal (head) and C-terminal (tail) domains. Lamins self-assemble into higher-order structures whose basic subunit is a coiled-coil dimer formed by in parallel and in register interactions (Stuurman et al., 1998; Herrmann and Foisner, 2003). Lamins A, B1, and B2 are expressed as prelamins that require wide-ranging posttranslational modifications of their carboxy-terminal –CAAX box to become mature lamins (Rusinol and Sinensky, 2006). Maturation of prelamins starts with the farnesylation of the cysteine residue at C-terminal of the protein by a farnesyltransferase (Lutz et al., 1992; Zhang and Casey, 1996), followed by the removal of the –AAX by a CAAX prenyl protease and by carboxymethylation of the carboxy-terminal cysteine (Winter-Vann and Casey, 2005). As opposed to B-type lamins, which remain permanently farnesylated and carboxymethylated, an

additional 15 amino acids are removed from the carboxyl terminus of farnesylated/carboxymethylated prelamin A by Zmpste24/FACE1, producing the mature lamin A (Corrigan et al., 2005). Lamin C, which is 74 residues shorter than mature lamin A, does not possess a –CAAX box and therefore is not farnesylated or otherwise modified.

Regarding their function, lamins play an overall scaffolding role and have been implicated in several processes including the maintenance of proper nuclear architecture, regulation of transcription, DNA replication and repair.

First of all, the lamins provide a structural framework for the nucleus playing a fundamental role in the determination and maintenance of cell shape and mechanical properties. In fact, cells either deficient in lamins or expressing mutant lamin proteins often contain misshapen nuclei (Ostlund et al., 2001; Vigouroux et al., 2001; Muchir et al., 2003; Goldman et al., 2004). Lamins interact with chromatin either directly or through histones and other lamin-associated proteins, such as lamin B receptor (LBR),

heterochromatin protein 1 (HP1), BAF, emerin, inner nuclear membrane protein MAN1, and several LAP2 isoforms (Wilson and Foisner, 2010). They also interact with different transcription factors that affect cellular proliferation, differentiation and apoptosis (Prokocimer et al., 2009; Wilson and Foisner, 2010). A-type lamins can modulate cell signaling through several mechanisms, for example, by sequestering transcription factors in inactive complexes or modulating post-translational modifications and degradation (Andres and Gonzalez, 2009; Dechat et al., 2010; Wilson and Berk, 2010; Wilson and Foisner, 2010).

Mutations in the lamins affecting their function generate a wide range of disorders referred to as laminopathies and that are often associated with severe loss in the structural integrity of the nucleus and with chromatins organizational defects (Capell and Collins, 2006). Laminopathies can be tissue-specific or systemic disorders and are divided in primary laminopathies when they are caused by mutations in LMNA gene or secondary laminopathies when genes encoding proteins with structural and/or functional relationship

with lamin A/C are mutated. As described previously the effects of LMNA mutation can be tissue specific, one example is muscular dystrophies as Emery-Dreifuss muscular dystrophy (EDMD) a LMNA-related myopathies (LMs) in which striated muscles are affected (Lattanzi et al., 2016). Adipose tissues are affected in lipodystophies such as Familial partial lipodystrophy type 2 (FPLD2).

Systemic laminopathies refer to a group of progeroid syndromes that includes Hutchinson-Gilford Progeria Syndrome (HGPS), restrictive dermopathy (RD), mandibuloacral dysplasia (MAD), and atypical progeroid syndrome (APS). However, HGPS is one of the most dramatic and prominent LMNA associated diseases (Zhang et al., 2011). This is a rare, sporadic, multi-system disorder characterized by features of premature aging, with most affected subjects dying in the second decade from cardiovascular disease (Dechat et al., 2008). The HGPS mutation is often a de novo C=>T transition that exposes a cryptic splice site, which generates the permanently farnesylated Δ50 variant of lamin A, known as

progerin, which acts as dominant negtive mutstion (Eriksson et al., 2003; Mendez-Lopez and Worman, 2012). The expression of progerin causes early cell senescence, dysmorphic nuclei, abnormal intranuclear chromatin distribution, redox defects, DNA damage and telomere attrition (Scaffidi and Misteli, 2006; Kubben et al., 2016). Since HGPS cell phenotype involves these multiple pathways, which are also intertwined, the interpretation of the disease is challenging also at the molecular and cellular level, and the identification of successful therapeutic strategies is complex. Moreover, it was found that in APS mutations in LMNA gene doesn't induce progerin production cause progeria too (Doubaj et al., 2012).

MAD is a rare disorder characterized by postnatal growth retardation, craniofacial features, and skeletal and cutaneous manifestations (Yang et al., 1971). The most common genetic defects are homozygous missense mutations in the LMNA (MADA) or ZMPSTE24 genes (MADB) (Lattanzi et al., 2016).

The telomeric protein AKTIP interacts with A- and B-type lamins and is involved in DNA metabolism

Recently in the laboratory where I have done PhD has been identified and partially characterized the accessory telomeric protein AKTIP, encoded by the human AKTIP gene. As reported in the literature this gene is the homologue of the Ft1 (Fused Toes 1) gene in mouse and pendoline (peo) of Drosophila (Cenci G et al., 2015). AKTIP is located on long arm of chromosome 16 (16q12.2) and codes for a protein of about 33 KDa, that belongs to the family of ubiquitine E2 variant proteins (UEVs) (Ye and Rape, 2009). UEVs are similar to E2 binding proteins ubiquitin (UBCs), but lack the residue corresponding to cysteine catalytic action necessary for the transient interaction between the E2 protein e ubiquitin itself (Ye and Rape, 2009). Recently we demostrated a robust structure similarity of AKTIP with the protein TSG101, another ubiquitin E2 variant protein, known to locate at the midbody and acting as part of the ESCRT-I complex, together with VPS37, VPS28 and MVB12 or UBAP1, to control membrane

scission, possibly via ubiquitylation (Bishop and Woodman, 2001; Teo el al., 2004; Carlton, 2010; Schoneberg et al., 2017).

Searching for homohlogues and orthologues into the three-dimensional structure protein data bank (PDB) we retrieved ESCRT human TSG101 and Saccharomyces cerevisiae VPS23 proteins to be top hits: TSG101 with estimated probability (EP) equal to 98.09% (E-value: 6.3E-7), while VPS23, the yeast orhtologue of TSG101, with EP equal to 98.48% (E-value: 1.8E-8) (Figure 3) (unpublished).

Functionality AKTIP directly binds the shelterin proteins TRF1 and TRF2 and interacts with the DNA replication factors PCNA and RPA70. AKTIP deficiency generates the activation of the DNA damage pathway, the accumulation of DNA damage foci at telomeric and non-telomeric DNA, of multiple telomeric signals and sister telomere associations that are hallmarks of defective telomere replication (Burla et al., 2015). In mice, Ft1 reduction causes prematurely aging defects that are partially rescued by reducing the expression of the DNA damage sensor p53 (La Torre

et. al, 2018). In addition to this, it was described that AKTIP interacts also with HOOKs, a group of proteins associated with vesicles that belong to the autophagy pathway, which, in turn, is related to the ESCRT machinery and depends on ubiquitination for selection of cargoes (Xu et al., 2008; Li et al., 2015).

Latly, AKTIP shows a peculiar intracellular distribution: in interphases cells is located, as discrete foci, both in the cytoplasm and in the nucleus. AKTIP is especially enriched at nuclear envelope, where interacts with A and B-type lamins. AKTIP depletion affects negatively A type lamin expresion and recapitulate several progeroid traits such as misshaped nuclei and loss of correct chromatin distribution. Additionally we observed that AKTIP is mislocated in cells from LMNA-mutations associated progeroid patients (Burla et al., 2015; 2016). Collectively these data suggest that AKTIPP is a new player in lamin-related processes and cellular senescence (Burla et al., 2015; 2016). In mitosis AKTIP is located at spindle matrix in metaphase and then, in anaphase is enriched at the bridge structure

connecting the two newly formed cells, called midbody (Burla et al., 2016).

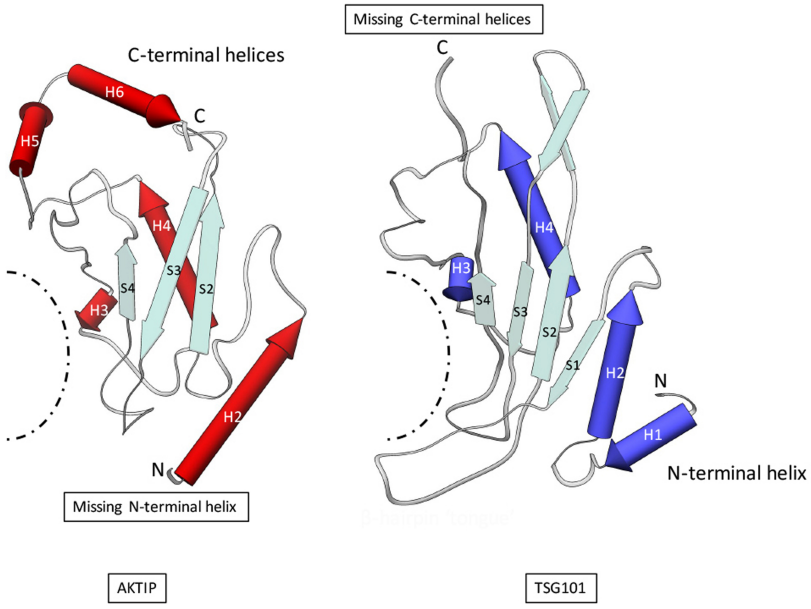

Figure 3: AKTIP shows structure similarity with the ESCRT-I protein Tsg101. A tridimensional molecular model reconstruction for AKTIP (left) and TSG101 (right).

AIM OF THE PROJECT

The laboratory where I carried out my PhD characterized AKTIP (in human, Ft1 in mouse) as a new shelterin-interacting protein. AKTIP is a new factor enriched at the nuclear envelope, controlling telomere function and genome stability (Burla et al., 2015; 2016). In addition to the localization at NE, it was recently demonstrated that AKTIP localize at midbody during cytochinesis (Burla et al., 2016).

The general aim of my PhD project was discover its role at the midbody and to expand and deepen our understanding of the function of AKTIP at NE.

The midbody is a transient structure that provides a platform for the recruitment and organization of many proteins that regulate the abscission. To complete cytokinesis, cells need to cut the midbody and this event is operated by ESCRTs (Carlton et al., 2010; Schoneberg et al., 2017). Building on the fact that AKTIP has multiple striking similarities with ESCRTs, indeed AKTIP interacts with vesicle factors, as HOOK (Xu et al., 2008), it is

enriched at the nuclear envelope and at the midbody (two ESCRT operated sites) (Burla et al., 2016). AKTIP belongs to the same family of ESCRT-I TSG101 with which AKTIP shares robust structure similarity, we decided to investigate AKTIP function at the midbody from an ESCRT perspective.

To obtain insights into the role of AKTIP at the midbody, we carried out a higher resolution microscopy analysis to better understand its localization. The structured illumination microscopy (SIM) allowing nanometer scale resolution of molecular complexes (Schermelleh et al., 2010) and had already used to interpret ESCRT organization and function (Elia et al., 2011). In addition to this, we performed biochemistry to investigate AKTIP interaction with a panel of known ESCRT factors. We also performed RNA interference in order to study what occurs at midbody after AKTIP downregulation.

Concerning AKTIP at nuclear periphery, we previously described that AKTIP interacts with A and B types lamins and its downregulation triggers a premature aging phenotype both at

cellular level and at organismal level (in a mouse model knocked down for its murine homologue Ft1) recalling those of progeroid patients with mutations in LMNA gene (Burla et al., 2016; La Torre et. al., 2018). The lamins are the major architectural proteins of the cell nucleus and line the inside of the nuclear membrane, where they provide a platform for the binding of proteins and chromatin and confer mechanical stability (Dittmer and Misteli, 2011).

Here we focused our attention on AKTIP relationship with lamins both in physiological and pathological conditions. We determined the spatial organization of AKTIP at NE respect to the B-type and A-type lamins using SIM. We also analysed the localization of AKTIP in human primary fibroblasts (HPFs) derived from LMNA-mutated patients in order to understand if and how AKTIP delocalization could contribute to the pathological phenotype.

RESULTS

AKTIP associates with the spindle apparatus during mitosis

Previous works have shown that AKTIP was enriched at the nuclear rim where co-localizes with A and B-type lamins. In addition AKTIP was reported also to have another peculiar localization during mitosis: at the midbody structure in the cytokinesis (Burla et al., 2015; 2016). This localization was interesting and prompted us to better examine the subcellular localization of AKTIP in cells undergoing mitosis and investigate its possible mitosis-associated function.

First the localization of endogenous AKTIP was depth analyzed in HeLa cells throughout mitosis using confocal microscopy. As shown in Figure 4A AKTIP is clearly detectable at the nuclear rim in interphase cells where it also has a cytoplasmic localization. The nuclear rim association is then lost throughout the mitosis and only acquired again in early cytokinesis, in conjunction with the reforming nuclear lamina. Once the nuclear envelope breaks apart during prophase and cells undergo mitosis AKTIP disaggregates

and returns to be again detected at the centrosome in prometaphase, along the microtubules in metaphase and at the spindle midzone during Anaphase B. During abscission, the late stages of cytokinesis, AKTIP clearly accumulates at the midbody.

The specificity of AKTIP localization at midbody was verified and validated by immunofluorescence using an anti-Flag antibody in HeLa cells transfected with plasmids encoding for the AKTIP-FLAG, also in this case we observed AKTIP at the center of the intercellular bridge (Figure 4B). In addition we tested the specificity of this localization by immunofluorescence in AKTIP depleted cells following LV-shAKTIP transduction. Only 47% of shAKTIP-treated cells are positive for staining with AKTIP at the midbody as opposed to 91.7% of ctr cells (Figure 4C-D).

Altogether, these results confirm the presence of AKTIP at the midbody suggesting a possible mitosis-associated function.

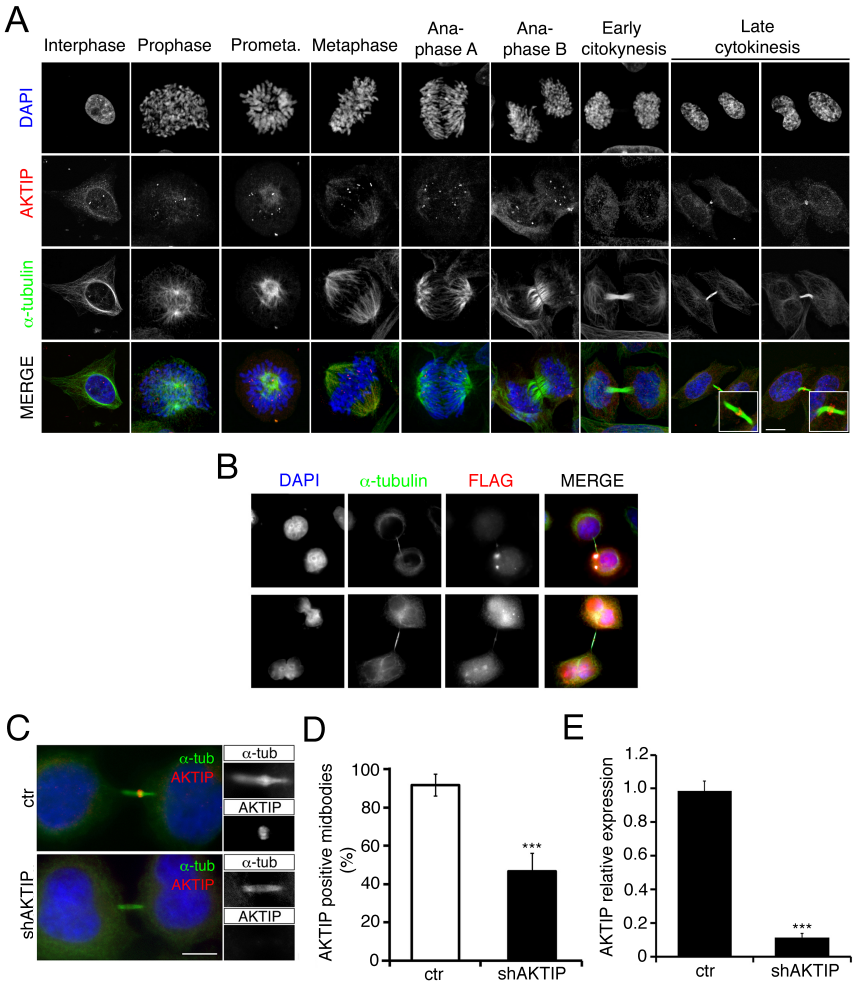

Figure 4: AKTIP is associated with the spindle apparatus during mitosis. (A) Distribution of endogenous AKTIP in HeLa cells during cell cycle progression. HeLa cells were stained with anti-AKTIP (red), anti-α-tubulin (green) and, to visualize DNA, with DAPI (blue). Scale bar, 5 μm. (B)

Immunostaining of AKTIP in AKTIP-FLAG expressing HeLa cells with an anti-FLAG antibody (red), anti-α-tubulin (green) and, to visualize DNA, with DAPI (blue). (C-D) Immunofluorescence analysis (C) and its quantification (D) showing that only 47% of shAKTIP-treated cells are positive for staining of AKTIP at the midbody as opposed to 91.7% of ctr cells (***$p < 0.001$; Student's t-test; 60 midbodies analyzed per condition). (E) AKTIP mRNA levels determined by Q-PCR in HeLa cells 7 days after LV transduction. AKTIP mRNA level, in interfered cells, is significantly reduced compared with control (***p , 0.001 in Student's t-test from three independent experiments).

AKTIP forms a ring-like structure at the center of the midbody in mid and late cytokinesis

In order to refine the characterization of AKTIP properties, we determined the spatial organization of the AKTIP at the midbody at different time points of cytokinesis by SIM.

HeLa cells were stained with anti-AKTIP and anti-α-tubulin antibodies and SIM images were 3D reconstructed (Figure 5). As previously described, we subdivided midbody stages into early, mid, late and cut basing on the tubulin bridge dimention (Elia et al., 2011). In the early stage, the midbodies is large and the tube is symmetric with respect to the central zone (dark zone), while in the mid phase, the microtubules are packaged into a structure that is still symmetric with respect to the darck zone but has a lower diameter. Late stage midbodies are recognized by their asymmetry and for the presence of the constriction site and the abscission is characterized by acute narrowing of one side of the midbody bulge followed by microtubule breakage and membrane cutting. Narrowing and scission of the other side of the midbody bulge then

occurs, leaving a midbody remnant dissociated from both daughter cells (cut stage) (Elia et al., 2011). In the early stage, AKTIP was detected as multiple spots on the microtubules of the midbody with an enrichment plane close to the center of the structure (Figure 5A). In the mid stage, the spots on the midbody arm were almost absent, while AKTIP formed a super-molecular structure around the central area of the microtubule tube. In late midbodies, the AKTIP structure lost its regularity. When the 3D image of AKTIP is rotated (Figure 4B), is clearly visible how AKTIP forms a ring-like structure residing at dark zone of midbody. The AKTIP ring has an average inner and outer diameter of 1.03 μm and 1,86 μm (n = 8), respectively (Figure 5C).

This observation was consistent with the previous immunolabeling results (Figure 4A) describing AKTIP midbody localization, but reveal new insight in its spatial organization.

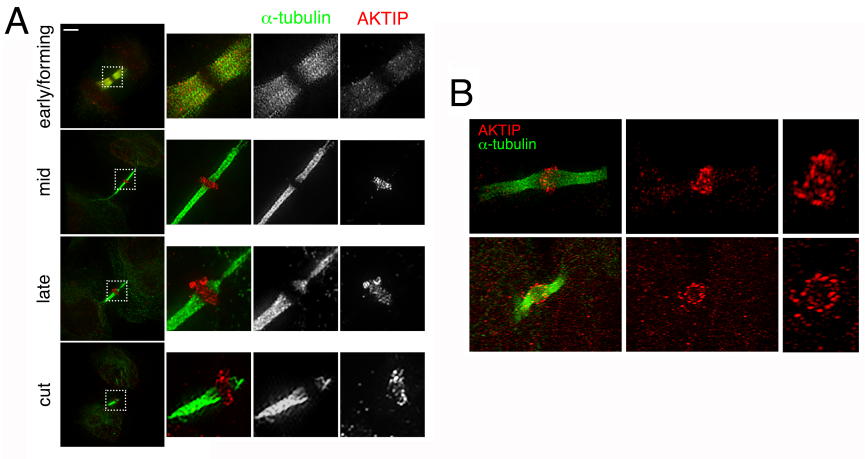

Figure 5: Spatial organization of AKTIP in the intercellular bridge of dividing cells. (A) HeLa cells were stained with anti-AKTIP (red) and anti-α-tubulin (green) antibodies and imaged by SIM system. Rappresentative images of cells at different cytokinesis stages show how AKTIP forms a ring-like structure surrounding the microtubules at the center of the midbody in mid and late cytokinesis. (B) The panel shows (from left to right) a 3D recostraction of merged AKTIP and tubulin (scale bar 2 µm); the same 3D view enlarged and rotated 90°, and used to measure ring size. The ring is, on average, 1,03 µm in its inner diameter and 1,86 µm in his outer diameter.

AKTIP have binding partners involved in cytokinesis

In silico data point to a connection of AKTIP with the ESCRT member TSG101 and with others ESCRT machine compartments. Indeed AKTIP shere a robust structure similarity with TSG101, anpther UEV protein (unpublished). To investigate this further, we probed in vivo AKTIP interaction with a panel of known ESCRT factors, including TSG101 and its partner protein VPS28.

To investigate this in vivo AKTIP was cloned EcoRI/NotI into pHB18 fused to DNA activation domain or pGBKT7 fused to DNA binding domain and screened in a yeast two hybrid assay against ESCRT components in pHB18 or pGBKT7. This analysis showed specific AKTIP interaction with VPS28 (Figure 6A).

To confirm, in mammalian cells, the interaction of AKTIP and VPS28 obtained in yeast cells, we also perfomed a GTS pull-down in 293T cells. VPS28 was cloned as GST-fusion protein and 293T cells were co-transfected with control GST or GST-VPS28 and MYC-AKTIP. Figure 6B demonstrate that MYC-AKTIP was proficiently precipitated by the fusion protein GST-VPS28, but not

by the GST protein *per se*. The interaction was further confirmed by GST pull-down assay using HA-AKTIP probed in 293T cells onto GST-VPS28 (Figure 6C). Also in this case HA-AKTIP was efficiently retained by GST-VPS28 but not by the empty GST.

Altogether these data reveal that AKTIP has substantial structural similarity with the ESCRT-I member TSG101 and interacts with VPS28.

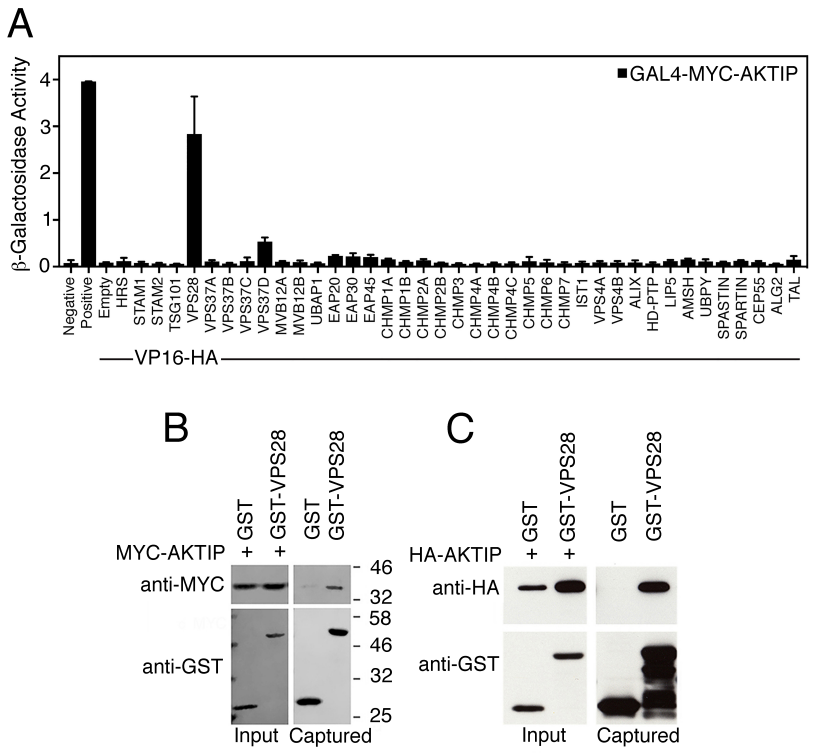

Figure 6: AKTIP has binding partners involved in cytokinesis. (A) AKTIP fused to the Gal4 DNA binding domain was tested for interactions with the human components of ESCRT-I, -II, -III, and ESCRT-III associated proteins fused to the VP16 activation domain by yeast two hybrid assays. Error bars indicate the SD from the mean of triplicate measurements. β-Gal, β-galactosidase; O.D., optical density. (B-C) GST pull-down showing that AKTIP interacts with VPS28 but not with GST alone. Cell lysates prepared from 293T

cells expressing MYC-AKTIP (B) o HA-AKTIP (C) were used for GST pull-down assay with GST and the fusion protein GST-VPS28. The pull-down products analyzed with MYC and HA antibodies.

AKTIP shows a close spatial proximity with ESCRT-III factors at the midbody in late cytokinesis

Overall the reported data, indeed its peculiar localization, the similarity with TSG101 and the interaction with VPS28, connect AKTIP to the ESCRT complexes.

To investigate whether AKTIP localization was temporally and spatially linked to subunits of the ESCRT machine we analysed the relative localization of AKTIP and ESCRT members. We focused on ESCRT-III CHMP4B, CHMP2A and IST1 which are recruited at the midbody by ESCRT-I and -II complexes for abscission (Carlton et al., 2008).

Endogenous CHMP4B, CHMP2A and IST1 distribution was alredy defined with high resolution microscopy showing that they localize at the midbody: form first they a double ring at either side of the central dark zone, then they expand into helices and spirals that narrow down to the incipient site of abscission (Gromley et al., 2005; Wollert et al., 2009; Elia et al., 2011; Goliand et al., 2018).

To directly resolve the spatial organization of AKTIP and others ESCRT-III protein at the midbody at different stages of abscission we used SIM system (Figure 7).

Consistently with previous description, we observed that in early forming midbodies the signal of both AKTIP and IST1 was not yet organized in a super-structure. In mid stage, both AKTIP and IST1 had the characteristic ring shaped super-molecular structures. The two IST1 rings typically side-packaged the central, single, ring of AKTIP at the center of the midbody. In late-to-cut stages, IST1 spirals became apparent and AKTIP progressively lost its circular organization. After abscission, in midbody remnants, both the AKTIP and IST1 signals were reduced (Figure 7A).

We then analyzed images of the two other ESCRT-III subunits, CHMP4B (Figure 7B) and CHMP2A (Figure 7C). In doubly anti-AKTIP and anti-ESCRT-III stained cells AKTIP ring was in between the two circles composed by these ESCRT-III subunits in mid stage. In late stages, the ESCRT-III subunits spiralized

towards the constriction site and AKTIP started to lose its structural regularity.

In addition, AKTIP apparently organizes at the midbody very similarly to ESCRT-I TSG101 partnering protein VPS36. Indeed, VPS36 was shown to localize as a ring at the center of the midbody, then extending in late cytokinesis towards the constriction site (Elia et al., 2011; Goliand et al., 2018).

Altogether these results indicate close spatial proximity of AKTIP with ESCRT-III factors at the midbody in late cytokinesis, strengthening the idea the AKTIP has a role durining cell abiscission.

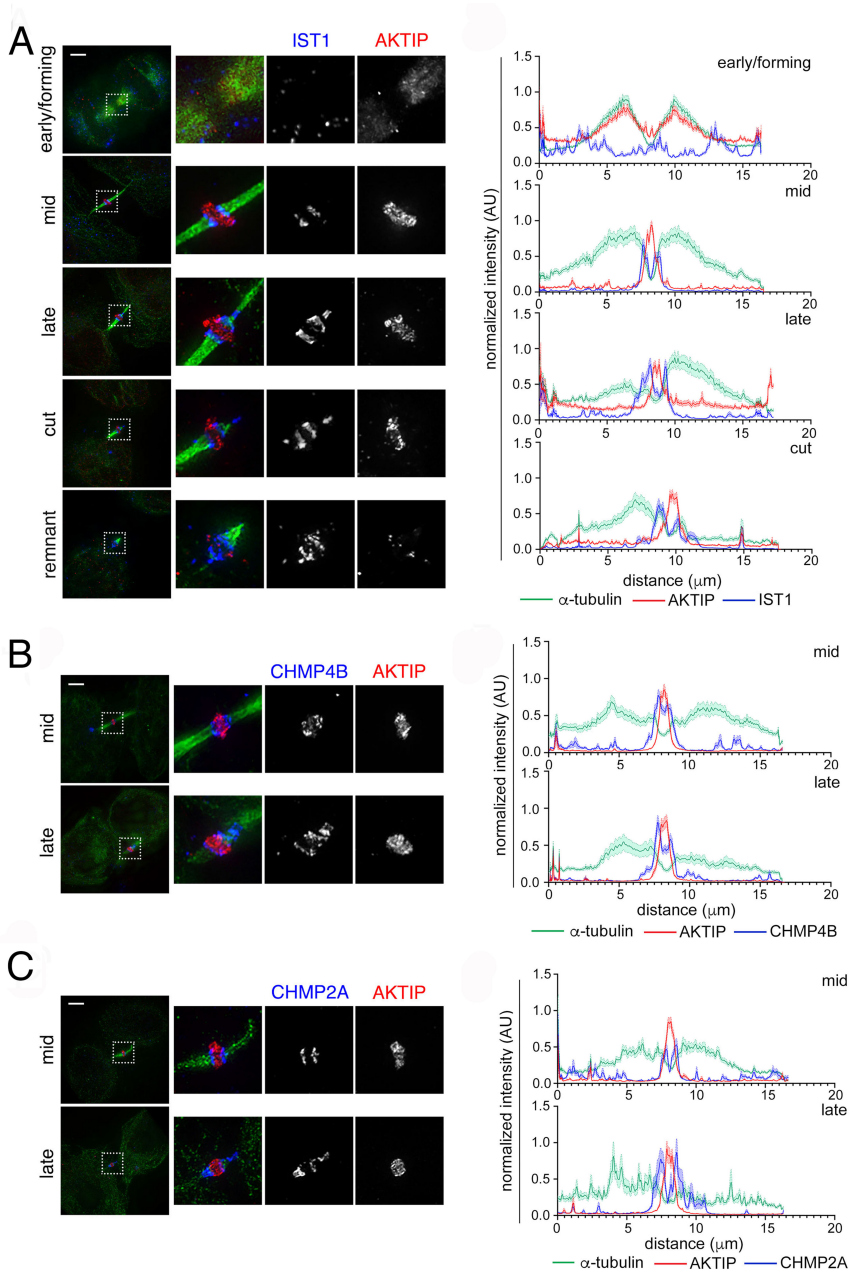
A
IST1
AKTIP
early/forming
mid
late
cut
remnant
normalized intensity (AU)
distance (μm)
α-tubulin
AKTIP
IST1
B
CHMP4B
AKTIP
CHMP4B
C
CHMP2A
AKTIP
CHMP2A

Figure 7: Spatiotemporal distribution of ESCRT-III proteins and AKTIP at the midbody. (A-C) Localization of AKTIP and IST1 (A), CHMP2A (B) and CHMP4B (C) in different stages of cytokinesis. HeLa cells were stained with α-tubulin (green), AKTIP (red) and ESCRT-III (blue) antibodies and imaged by SIM system. Representative 3D-SIM images of localization of AKTIP and ESCRT-III proteins showing AKTIP ring located between the ESCRT-III double ring, flancking the centre of the midbody, formed ESCRT-III proteins (scale bar 2 μm). Plots show the mean pixel intensity of AKTIP (red) and IST1 (A) or CHMP4B (B) or CHMP2A (C) (blue) and α-tubulin (green) across the width of the midbody.

AKTIP cooperates for the correct recruitment of the ESCRT-III component

It is well known that ESCRT complexes coordinate membrane abscission. In a working model of this process ESCRT-I proteins (directly or indirectly) recruit ESCRT-III complex that leads to the cleavage of the membrane neck (Carlton et al., 2008).

Given the links of AKTIP with the ESCRT-I TSG1 and the spatial proxity between AKTIP and ESCRT-III at the midbody, we decided to investigate the impact of AKTIP on ESCRT-III recruitment at the midbody.

We immunostained control and AKTIP depleted HeLa cells with anti-IST1, anti-CHMP2A and anti-CHMP4B antibody and checked their localization in cytokinesis. In cells with reduced AKTIP expression, the localization at midbody of CHMP2A and CHMP4B (Figure 8A-B) were only modestly affected, with more than the 70% of shAKTIP cells positive for CHMP2A or CHMP4B signal (Figure 8D). On the contrary, IST1 is not always present at the midbody after AKTIP depletion (Figure 8C). Indeed in

shAKTIP cells IST1 localization at the midbody was strongly impaired, since IST1 signal dropped from 80% positivity in controls to 25% in shAKTIP cells (Figure 8D).

Altogether these data suggest a role for AKTIP in abscission through the recruiment of IST1 at midbody.

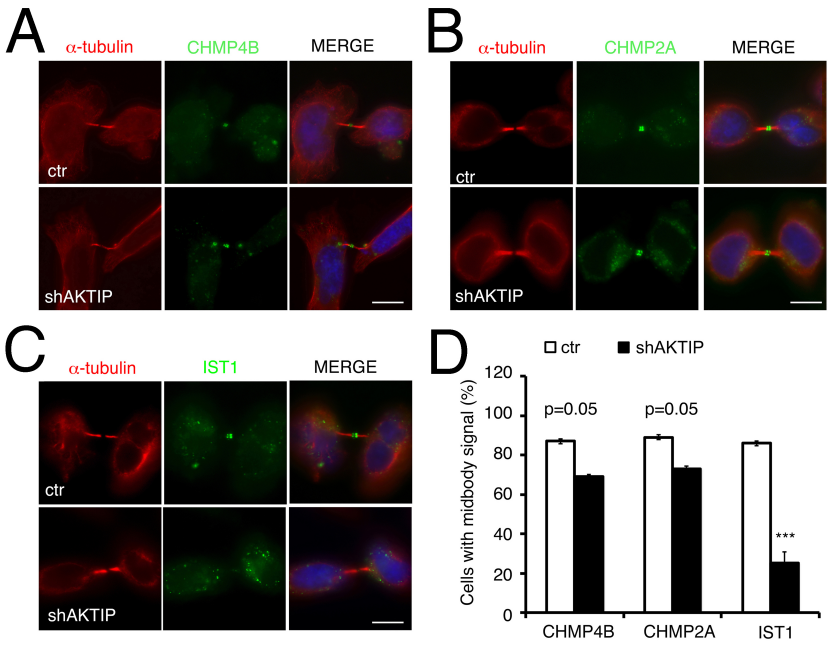

Figure 8: AKTIP-dependent localization of ESCRT-III components. (A-C) Localization of IST1 (A), CHMP2A (B) and CHMP4B (C) in Lv-shAKTIP and control cells by immunofluorescence (IF) staining with antibodies against markers (green) and α-tubulin (red). (D) Quantification of cells from (A-C) displaying defects in the localization of IST1, as opposed to CHMP2A and CHMP4B, markers at the midbody in AKTIP knowdown cells. Scale bars, 5 µm. *p < 0.05; Student's t-test; 60 midbodies analyzed per condition.

Loss of AKTIP is associated with cytokinesis defects

Previous studies have shown that impaired ESCRT function induces cytokinesis defects as regression of the cleavage furrow or to formation of a persistent connection between the two daughter cells. these can be divided in (Wheatley and Wang, 1996; Canman et al, 2000; Straight and Field, 2000).

Given the connection between AKTIP and IST1, we then asked whether the observed AKTIP impact on IST1 recruitment would affect cell cycle progression and cytokinesis. Indeed IST1 is able to recruit the ESCRT-III associated AAA-ATPase Spastin to the midbody (Agromayor et al 2009, Adell et al 2011), where it coordinates the last events necessary for abscission.

We first explored whether AKTIP depletion affected cell division progression performing live cell microscopy using HeLa cells stably expressing mCherry fluorescently tagged α-tubulin. AKTIP reduction was achieved by siRNA transfection (Figure 9D). Live cell imaging revealed that AKTIP reduction caused cells to extend the abscission stage of cytokinesis and remain tethered together

through their midbody for longer times respect to control cells (Figure 9A-C). In siAKTIP cells the duration of abscission after telophase was longer then in the control cells. Indeed the average time at midbody stage was 114 min ± 14.4 in AKTIP reduced cells, while it was 74 ±4.5 min in controls cells (Figure 9B), indicating that the intercellular bridge persisted longer when AKTIP was reduced. In siAKTIP cells the midbody stage persist more than in control cells (Figure 9C).

Analyses on fixed cells confirmed that AKTIP reduction caused cytokinesis defects. Indeed when we immunostained control and shAKTIP cells with α-tubulin, compared with control cells, shAKTIP samples showed an increase in the number of binucleated cells (Figure 9E-F).

Altogether these data suggest that AKTIP by localizing at midbodies intercepts the ESCRT complex with particular impact on IST1 recruitment which in turn contributes to correct cytokinetic function.

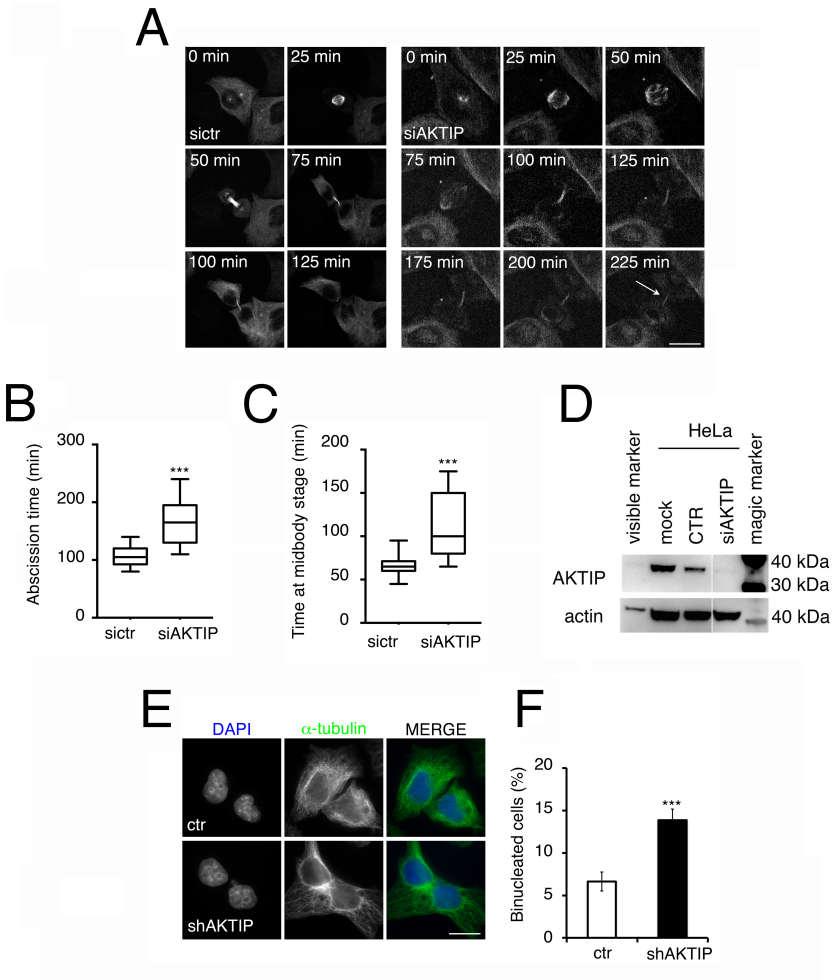

Figure 9: Silencing of AKTIP is associated with cytokinesis defects. (A) Selected frames from time-lapse microscopy of HeLa cells stably expressing mCherry-α–tubulin transfected with ctr (left) or AKTIP (right) siRNA. The arrow point to an example of two cells that remain still connected, showing a

delay in cytokinesis. Elapsed times are provided in each panel. Images were recorded every 5 min, starting 48h after siRNA transfection. (B-C) Quantitative analysis of time-lapse microscopy. The amount of time from prometaphase to abscission (B) and from telophase to abscission (C) was measured. (D) Western blotting showing the reduction of AKTIP expression in HeLa cells treated with siRNA for AKTIP respect to the control cells (E) Representative images of binucleated cells observed in shAKTIP cells are shown with DAPI in blue and α-tubulin in green. scale bar, 10 μm. (F) Quantification of binucleated cells in control and AKTIP depleted cells (shAKTIP) (**$p < 0.01$, ***$p < 0.001$; Student's t-test).

AKTIP localizes at nuclear rim where shows a close spatial proximity with lamins

The NE consists of two concentric membranes — the outer (ONM) and inner (INM) nuclear membranes — nuclear pore complexes (NPCs) and an underlying nuclear lamina network (Gruenbaum et al., 2005). Our previous results showed that AKTIP has a peculiar intracellular distribution including a punctate enrichment at the nuclear rim where it partially colocalizes with lamins (Burla et al., 2016).

In order to refine the characterization of AKTIP properties, we determined the spatial organization of AKTIP at nuclear envelope (NE) respect to the B-type (Figure 10 A-C) and A-type lamins (Figure 10 D-F) using SIM. In addition, using SIM, we also analyzed the localization of AKTIP rispect to NPC, visualized with antibody against TRP a compinent of NPC. A- and B-type lamins form separate filamentous networks in the lamina of somatic cells. Imaging of the lamin structure in somatic cells has proven to be problematic due to the complex organization of the somatic cell

nuclear envelope and the tight association of chromatin fibers with the lamina. It is known that A- and B-type lamins form different types of filaments in separate intranuclear compartments. B-type lamins formed irregular wavy filaments associated with intranuclear membrane structures. In contrast, A-type lamins formed thick multilayered assemblies of filaments (Goldberg et al., 2008). Moreover each type of lamin forms a distinct meshwork structure with a relatively small number of points of colocalization (Shimi et al., 2008).

Our reconstructed 3D-SIM images of double-labeled nuclei show that AKTIP is enriched at nuclear lamina as discrete foci, in a similar way of A-type lamins, indeed AKTIP has multiple co-localization points at NE with lamin A/C (Figure 10 D-F), but not with B-type lamins (Figure 10 A-C)

The colocalization of red (laminA/C) or blu (TRP) and green (AKTIP) spots was estimated by calculating the Paerson's colocalization coefficient (PCC). PCC is a standard statistical analysis designed to measure the strength of a linear relationship

between two variables, in this case fluorescent spots (Barlow et al., 2010). As shown in Figure 10I, AKTIP colocalizes strictly with A-types lamins but not with TRP.

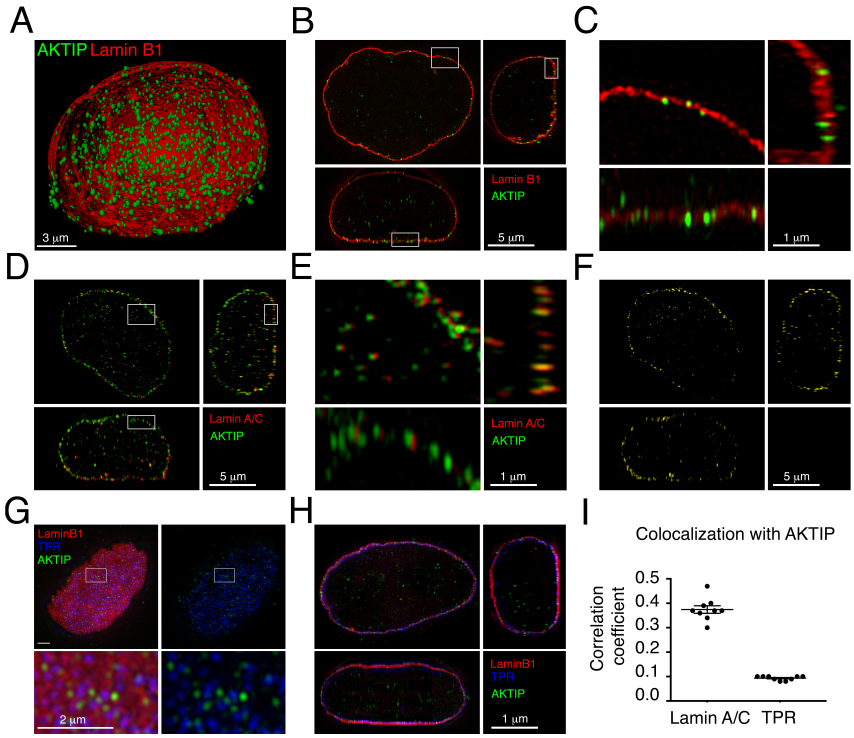

Figure 10: AKTIP localizes with lamin protein at NE in NPC-indpipendent way. (A) 3D rendering of a HeLa cell nucleus from super resolution imaging data. The nuclear lamina (red) has been rendered partially to allow visualizing the position of AKTIP (green) within the nucleus, scale bars 3 µm. (B-E) Projection of an extended section of a wild type nucleus – view from orthogonal planes showing Lamin B1 (red) (B) or Lamin A/C (D) and AKTIP (green) staining. Enlargment section indicated by the white frames shown in panel B (C) or in panel (E). Scale bars 5 µm and 1 µm respectively. (F) Orthogonal planes revealing the colocalization of AKTIP and Lamin A/C are shown in yellow.

Scale bars 5 μm. (G-H) Simultaneous imaging of nuclear Lamina, NPC epitope and AKTIP by 3D-SIM. HeLa cells were immunostained with antibodies against Lamin B1 (red), TPR (blue) and AKTIP (green). Projection of five apical section (corresponding to a thickness of 0.5 mm). Scale bars 2 μm and 1 μm, respectively. (I) Colocalization analysis was performed using the Imaris Colocalization module. Colocalization between AKTIP and Lamin A/C in the experiment in (D) and colocalization between AKTIP and TRP (NCP) in the experiment in (G) was quantified using Paerson's colocalization coefficient. Data are shown as the mean ±SEM (n=9)

Defects in lamin A impair AKTIP localization at nuclear rim

Consistent with AKTIP distribution at NE, it was demostrated that lamins are among AKTIP interactors and mutations in lamis encoding gene impair AKTIP nuclear envelope localization. Addictionaly AKTIP downregulation triggers, both at cellular level and at organismal level (in a mouse model knocked down for its murine homologue Ft1) a premature aging phenotype recalling those of progeroid patients with mutations in LMNA gene (Burla et al., 2016; La Torre et al., 2018).

To investigate deeply the connection beetwen AKTIP and lamins, we first examine the relative localization at NE of AKTIP and both A-type and B-type lamins in HeLa cells expressing progerin. The HeLa cells were transfected with a construct for progerin expression, then doubly immunostained with anti-AKTIP and anti-lamins antibodies and analyzed by SIM (Figure 11).

It is known that progerin, a truncated form of lamin A, responsible for the HGPS, acts as a dominant factor and leads to multiple morphological difects of cell nuclei (Gordon et al., 2014).

As expected the 3D rendering of progerin expressing nuclei confirms that the over-expression of progerin leads to alterations in nuclear structure, and impaires the AKTIP localization at NE. In these cells AKTIP punctate pattern appeares more discontinuous than in controls, in which AKTIP is clearly detectable at nuclear rim (Figure 11 A-I).

The analysis of colocalization between AKTIP and Lamin A/C (Figure 11M) carring out calculating of PCC, highlight how in progein expressing nuclei AKTIP localization at NE has been distorted. Indeed the PCC is significantly reduced in progerin expressing cells respect to the control cells.

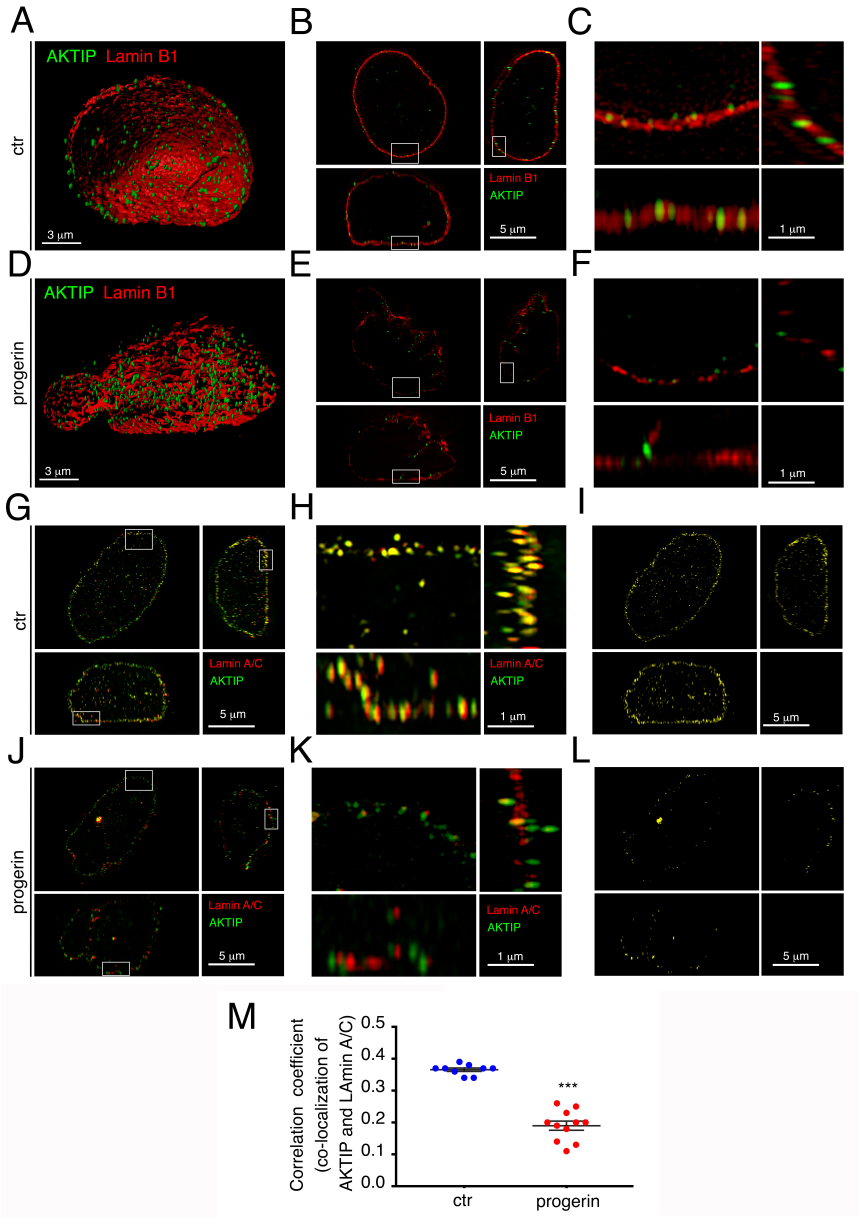
A
B
C
AKTIP Lamin B1
ctr
3 µm
Lamin B1
AKTIP
5 µm
1 µm
D
E
F
AKTIP Lamin B1
progerin
3 µm
Lamin B1
AKTIP
5 µm
1 µm
G
H
I
ctr
Lamin A/C
AKTIP
5 µm
Lamin A/C
AKTIP
1 µm
5 µm
J
K
L
progerin
Lamin A/C
AKTIP
5 µm
Lamin A/C
AKTIP
1 µm
5 µm
M
Correlation coefficient
(co-localization of
AKTIP and LAmin A/C)
0.5
0.4
0.3
0.2
0.1
0.0
***
ctr
progerin

Figure 11: AKTIP lost association with lamin A in progerin expressing cells. 3D rendering of ctr (A) and HeLa cells expressing progerin (D) from super resolution imaging data showing nuclear lamina (red) and AKTIP (green). Scale bar, 3 μm. Projection of an extended section of a wild type nucleus (B-C, G-H) and progerin expressing cells (E-F, J-K) – viewed from orthogonal planes showing Lamin B1 (red) (B, E) or Lamin A/C (G, J) and AKTIP (green) staining and (C, F, H, K) enlargment section indicated by the white frames shown in panel B (C), in panel E (F), in panel G (H) and in panel J (K). Orthogonal planes revealing the colocalization of AKTIP and Lamin A/C in ctr (I) or expressing progerin (L) cells, are shown in yellow. Scale bars 5 μm. (M) Colocalization analysis was performed using the Imaris Colocalization module. Colocalization between AKTIP and Lamin A/C was quantified using Paerson's colocalization coefficient. Data are shown as the mean ±SEM (n=9)

In addition we analysed also the localization of AKTIP in human primary fibroblasts (HPFs) derived form HGPS and EDMD2 patients (Figure 12).

In cells from HGPS patients, progerin accumulates at the inner membrane of the nuclear envelope and disrupts normal nuclear lamina organization leading to nuclear shape alteration, instead this nuclear altretion is less strong for EDMD2 cells.

We immunostained control and HGPS or EDMD2 cells with anti-AKTIP and anti-Lamin A/C or Lamin B1, and checked AKTIP localization at NE using SIM.

3D SIM images indicated that AKTIP in HGPS (Figure 12E-H), as opposed to controls cells (Figure 12A-D), is reduced at the NE, recalling the phenotype the we osperved in Hela overexpressing progerin (Figure 11). Indeed the peculiar AKTP punctate distribution at NE appeares more discontinuous in HGPS cells than in controls. This alteration of AKTIP localization is also confirmed by calculating of PCC between Lamin A/C and AKTIP (Figure

12M-P), which is significantly reduced in HGPS cells respect to the control cells.

To the contrar EDMD2 cells (Figure 12I-L) don't shown any altration of AKTIP localization at NE, in which AKTIP shows the same localizzation at the NE as control cells. Indeed, in EDMD2 cells AKTIP and lamins A/C colocalization was unaffected, while in HGPS cells was strongly impaired (Figure 12 M-P).

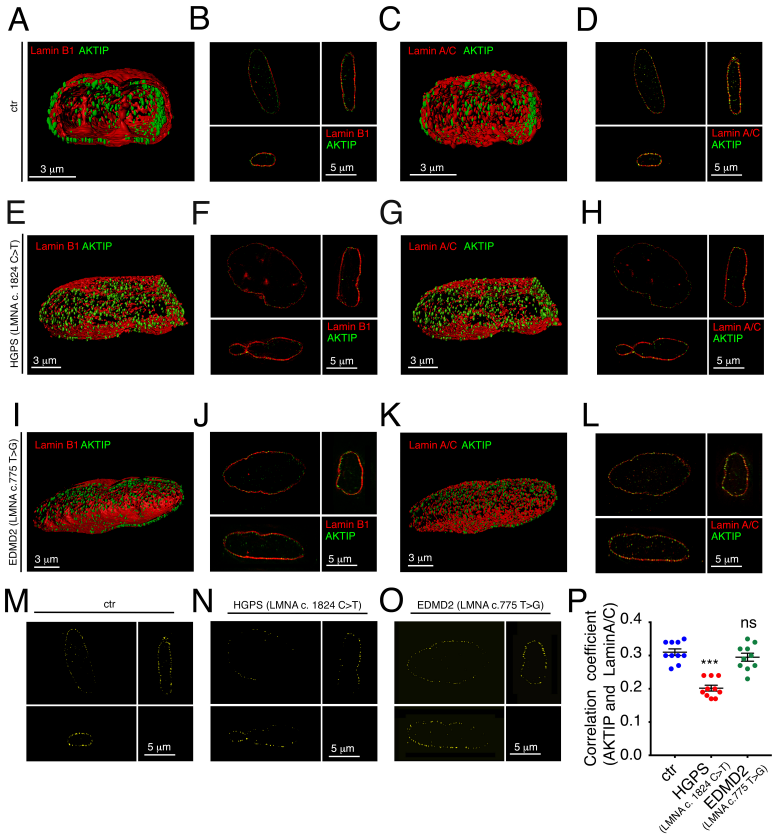

Figure 12: AKTIP association with Lamins in HGPS and EDMD2 cells. 3D rendering of ctr (A,C) HGPS (E,G) and EDMD2 cells (I,L) from super resolution imaging data showing nuclear lamina (red) and AKTIP (green). Scale bar, 3 µm. Projection of an extended section of a wild type nucleus (B,D), HGPS (F,H) and EDMD2 cells (J,L) – view from orthogonal planes showing Lamin B1 (red) (B, F, J) or Lamin A/C (D, H, L) and AKTIP (green) staining. Orthogonal planes revealing the colocalization of AKTIP and Lamin A/C in ctr (M), HGPS

(N) or EDMD2 (O) cells, are shown in yellow. Scale bars 5 μm. (P) Colocalization analysis was performed using the Imaris Colocalization module. Colocalization between AKTIP and Lamin A/C was quantified using Paerson's colocalization coefficient. Data are shown as the mean ±SEM (n=9).

AKTIP delocalization in lamin A mutant cells is connected with nuclear shape alteration

Besed on these different results obtained for AKTIP localization in HGPS and in EDMD2 cells, we speculate that the AKTIP abnormal localization can been linked to the nuclear shape alteration.

To test this hypotesis, we performed an extensive evaluation of AKTIP distribution in cells derived form patients carring different mutation in LMNA gene as HGPS, Atypical HGPS, EDMD2 and FPLD2 (Figure 13A).

We immunostained the cells with anti-AKTIP antibodies and analyzed its loclaizzazion related to nuclear shape alteration. As shonw in Figure 13 the immunofluorescence analysis and its quantification confirms that the mutation in LMNA gene leads to the delocalization of AKTIP and this localization is more severe more is the nuclear shape deformation (Figure 13 B-D).

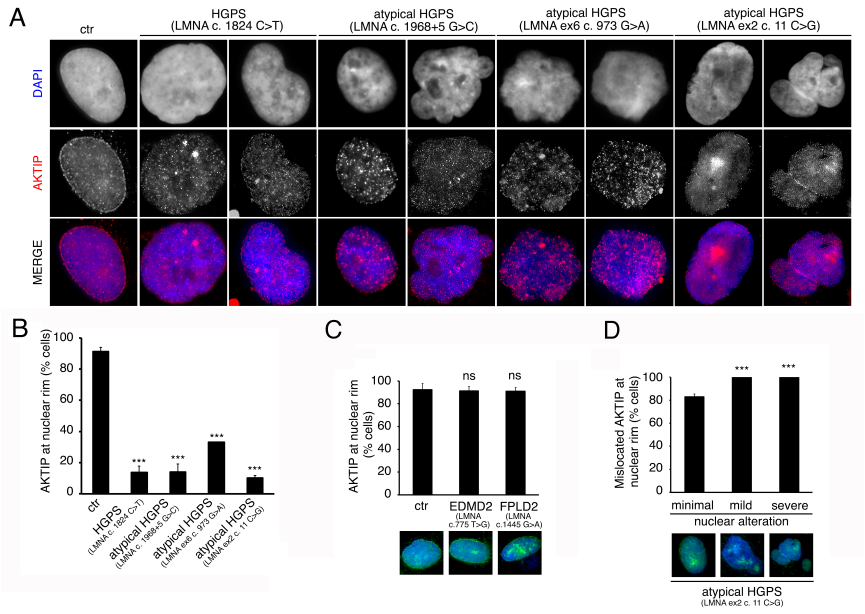

Figure 13: AKTIP delocalization in lamin A mutant cells is connected with nuclear shape alteration. (A) Distribution of endogenous AKTIP in ctr, HGPS and atypical HGPS cells. All type of cells were stained with anti-AKTIP (red) and, to visualize DNA, with DAPI (blue). (B-D) Immunofluorescence analysis showing that (B) lee of 20% of HGPS cells are positive for staining with AKTIP (monoclonal) at the NE as opposed to 90% of ctr cells or EDMD2 and FPLD2 cells (C) (***$p < 0.001$; Student's t-test; 200 cells analyzed per condition). (D) The delocalization of AKTIP increas with the severity on nuclear shape deformation (***$p < 0.001$; Student's t-test; 200 cells analyzed per condition).

DISCUSSION

The laboratory in which I carried out my PhD project recently discovered, a non-shelterin telomeric protein, known as AKTIP, which binds the shelterin proteins TRF1 and TRF2 and which deficiency generates telomere fragility by impinging on replication (Burla et al., 2015). AKTIP also interacts with lamins and its downregulation triggers a premature aging phenotype (Burla et al., 2016; La Torre et. al 2018). Another AKTIP peculiarity is its intracellular distribution: in interphases cells AKTIP is enriched, as discrete foci, at nuclear envelope. In mitosis AKTIP is located at spindle matrix in metaphase and then it is enriched in anaphase at the midbody (Burla et al., 2015; 2016).

The general aim of my PhD project was to discover role of AKTIP at the midbody and expand and deepen our understanding of its function at NE.

In the first part of my PhD work, we focused on AKTIP role at midbody. The midbody is a membrane structure enriched in microtubules, that connects the two daughter cells at the end of

cytokinesis. To complete cytokinesis cells need to cut the midbody and this event is operated by ESCRT complex (Carlton 2010; Schoneberg et al., 2017). The ESCRT machine is divided in four subfamilies, ESCRT type I, II and III and VPS4 and the ESCRT subunits are sequentially positioned at the midbody with a precise spatiotemporal scheme.

We start from different observations suggesting that AKTIP activity could be associated with the ESCRT complex. A first indication comes from the observation that AKTIP functions in vesicle trafficking (a process in which the ESCRT machine plays an important role) through the interaction with HOOKs (Xu et al., 2008; Li et al., 2015). The second indication comes from a bioinformatic search in the 3D structure data bank, which indicated that AKTIP has a strong homology with a member of the ESCRT machine, the ESCRT-I subunit TSG101 (unpublished). AKTIP and TSG101 belong to the same family of UEVs protein (Ye and Rape, 2009). UEVs are similar to UBCs, but lack the residue corresponding to cysteine catalytic action necessary for the

transient interaction between the E2 protein e ubiquitin itself (Ye and Rape, 2009). The mechanism of action of these proteins has not yet been fully understood. Lastly AKTIP are detected at two ESCRT operated sites (i.e. the nuclear envelope and the midbody). Here, we described by SIM that AKTIP forms a super-molecular structure around microtubules at the center of the midbody (dark zone) where the ESCRT complex is recruited and acts to finalize abscission (Elia et al., 2011; Karasmanis et al., 2019). The super-molecular structure of AKTIP has the shape of a ring with an average internal diameter around 1.03 μm and an outer diameter of 1.86 μm. This ring-like organization of AKTIP recalls that of ESCRTs and ESCRT associated factors. These factors form a series of circular structures in the dark zone. For example it has been so assessed that ESCRT-I TSG101 forms a double ring structure that is preserved till abscission (Goliand et al., 2014). ESCRT-III subunits, including CHMP2A, CHMP4B and IST1, are organized at first as double rings at the two sides of the ESCRT-I/II complex. In mid/late stage the organization of these ESCRT

subunits evolves into spiral structures with progressively smaller diameters towards which reach the constriction site (Elia et al., 2011; Goliand et al., 2018).

We also studied the temporal of AKTIP, in comparison with that of ESCRT-III proteins, at the midbody observing that the AKTIP super-molecular organization into a ring precedes the completion of ESCRT-III elements assembly. When the ESCRT-III elements have formed full circular structures, in the mid stage of abscission, the AKTIP ring is found at the center and in proximity with the ESCRT-III subunits IST1, CHMP2A and CHMP4B. In the late stages of abscission, when the spiral formed by the ESCRT III factors became evident, AKTIP super-molecular organization showed a loss of regularity. These data suggest that the AKTIP circular structure is likely needed in the first steps of abscission.

The proximity of AKTIP with ESCRT-III subunits and the temporal sequence of recruitment, suggested that AKTIP could influence ESCRT-III complex assembly. Indeed AKTIP reduction significantly impinged on ESCRT-III IST1 recruitment at the

midbody.

Based on these results we speculate that AKTIP, localizing at midbodies, intercepts the ESCRTs pathway with particular impact on IST1 recruitment which in turn contributes to correct cytokinetic function. Indeed it is known that IST1 is able to recruit during cytokinesis the ESCRT-III associated AAA-ATPase Spastin to the midbody, where it coordinates the last events necessary for abscission (Agromayor et al 2009, Adell et al 2011). In the case of AKTIP, the reduction of its expression had an impact on cell division. Cells with reduced AKTIP expression had significantly longer abscission times and were more frequently binucleated as compared to controls. These data indicate that AKTIP, most probably by its effect on IST1, contributes to cell division completion.

This hypothesis is further supported by the fact that we found an interaction of AKTIP with an ESCRT-I member, VPS28, in analogy with the TSG101. Since VPS28 bridges the ESCRT-I to the ESCRT-II complex (Carlton and Martin-Serrano; 2007), these

data suggest a pathway in which AKTIP is connected with ESCRT-II and then to ESCRT-III via VPS28.

In the second part of my PhD work, focusing on AKTIP at nuclear periphery, we studied its relationship with lamins both in physiological and pathological conditions. The nuclear lamina is a structure positioned between the nuclear envelope and the chromatin and has been involved in different processes ranging from nuclear architecture to DNA metabolism. Mutations in the lamin A/C encoding gene result in a wide range of rare diseases named laminopathies. The most widely studied, among them, is the Hutchinson-Gilford progeria syndrome (HGPS) (Butin-Israeli et al., 2012).

Using SIM we determined the spatial organization of AKTIP at nuclear envelope showing that AKTIP localized at NE in a close proximity with A-type lamins. It is known that A- and B-type lamins form a distinct meshwork structure with a relatively small number of points of colocalization (Shimi et al., 2008). Our 3D-SIM data highlight how AKTIP is enriched at nuclear lamina as

discrete foci, in a similar way as A-type lamins, indeed AKTIP has multiple co-localization points with lamin A/C, but not with B-type lamins. In order to investigate the connection between AKTIP and lamins more deeply, we perform an extensive evaluation of AKTIP distribution in cells derived from patients carrying different mutation in LMNA gene as HGPS, atypical HGPS, EDMD2 and FPLD2, by both high resolution and canonical light microscopy. As described before AKTIP localization is altered in HGPS and in atypical HGPS cells, as well as in cells overexpressing progerin, but not in EDMD2 cells. Moreover, we demonstrated that AKTIP abnormal localization can been linked to the alteration of the nuclear shape, as AKTIP mislocalization is more severe the more the nuclear shape is deformed.

Recently it was discovered that during interphase, ESCRTs operate also at NE, where it repairs nuclear envelope ruptures, thus maintaining cellular viability and protection of the genome (Denais et al., 2016; Raab et al., 2016; Robijns et al., 2016).

Recent work on IST1 has shown that this is recruited at the nuclear

envelope to seal the membrane of the daughter nuclei by CHMP7 (Vietri et al., 2015). Moreover, it was discovered that the ESCRT machinery is important in interphase nuclei, especially in fragility and stress prone conditions as in the presence of lamin A mutations (Olmos et al., 2015). CHMP7 facilitates the reparation of holes at the nuclear envelope and it is linked with HGPS nuclear defects (Denais et al., 2016; Raab et al., 2016). These reports highlighted ESCRT pathway as a new pathogenic mechanism for HGPS that deserve further investigations.

Here, we have evidence that AKTIP is a putative member of the ESCRT family. These results prompted us to speculate to AKTIP plays a role in combination with the ESCRT machine at the nuclear membrane and that the cellular phenotype of chromatin damage and cell cycle arrest that we observed in AKTIP depleted cells could be due to defects in nuclear envelope sealing processes, as happen in cells with reduced levels of CHMP7.

MATERIAL AND METHODS

Cell culture procedures and RNA interference

Human foreskin primary fibroblasts (HPFs) from healthy donors (provided by A. Orecchia, IDI, Rome, Italy) were used at early passages (from p5 to p10), unless otherwise specified. HeLa (ATCC CCL-2) cells, HeLa mCherry tubulin (Olmos et al., 2015) and HPFs were grown under standard culture conditions (37°C; 5% CO_2) in DMEM (Dulbecco's modified Eagle's medium; Life technologies) supplemented with 10% fetal bovine serum (FBS, Life Technologies) and 50 U/ml penicillin and streptomycin (Life Technologies).

For transient RNA interference, cells were cultured in 6-well dishes and transfected with 20 μM siRNA oligonucleotides using Lipofectamine 2000 (Life Technologies) following the manufacturer's protocol. Cells were collected or fixed 72 h post-transfection. AKTIP and Control siRNAs were ordered from Sigma (SASI_Hs01_0086240 for AKTIP and siRNA universal negative control #1-SIC001 for ctr).

AKTIP-FLAG-expressing HeLa cells were obtained by lipofectamine 2000 (Life Technologies) mediated transfection of the pCMV6-Entry-AKTIP-FLAG plasmid (OriGene) following the manufacturer's protocol.

HGPS and Atypical HGPS primary dermal fibroblasts cell lines were obtained from The Progiria Research Foundation (PRF) Cell and Tissue Bank. The HGPS cells were obtained from 8-year-old patient carrying the LMNA c.1824C>T heterozygous mutation. The Atypical HGPS cell lines were obtained from 6-year-old patient carrying the LMNA 1968+5G>C heterozygous mutation and form 8-months-old patient carrying the LMNA c.973G>A heterozygous mutation. Cell cultures were established and grown in DMEM (Life Technologies) supplemented with 15% fetal bovine serum (Life Technologies), 50 U/ml penicillin and streptomycin (Life Technologies). The experiments were performed on cells at p12. EDMD2 (obtained from a patient carrying the LMNA c.775T>G mutation), FPLD2 (obtained from a patient carrying the LMNA c.1445G>A mutation) and Atypical

HGPS fibroblasts (obtained from a patient carrying the LMNA c.11C>G mutation) were provided by G. Lattanzi, CNR, Bologna, Italy and maintained in culture in DMEM (Life Technologies) supplemented with 15% fetal bovine serum (Life Technologies), 50 U/ml penicillin and streptomycin (Life Technologies). Skin biopsies were obtained from patients and donors according to local and EU ethical rules following informed consent.

Lentiviral production, infection and selection

The LV-mediated RNAi was carried out using SIN (Self Inactivated) second-generation recombinant lentivectors. Briefly recombinant lentivectors were derived by the combined transfection of three elements: (1) a transfer vector encoding gene specific interfering sequences, (2) the packaging vector pCMV-dR8.74, and (3) the VSV-G envelope vector pMD2G and titrated for p24 antigen content as previously described (Burla et al., 2015). The transfer vector cloned into pLKO.1 (Sigma) was used to produce LV-shAKTIP (shAKTIP) and LV-scramble (control, ctr) as already described (Burla et al., 2015). The transfer vector

pCDHblastMCSNard OST-LMNAD50 (Addgene 22662) was used to produce LV-progerin (Pegoraro et al., 2009). The multiplicity of infection (moi) used for all experiments was 3pg p24/cell. Transductions were performed in complete medium supplemented with 8 µg ml-1 polybrene (Sigma). After viral addition, cells were centrifuged for 30 min at 1800 rpm at room temperature (RT), incubated for 3 h at 37 °C, and then transferred to fresh complete medium. Seventy-two hours post-infection, cells transduced with LVs obtained with pLKO.1-derived transfer vectors were subjected to selection in complete medium supplemented with 2 µg ml-1 puromycin (Sigma) and kept under these conditions for further analyses. Seventy-two hours post-transduction, cells transduced with LV-progerin were subjected to selection in complete medium supplemented with 10 mg/ml of blasticidin (Sigma) and kept under these conditions for further analyses

mRNA quantification

One-week post-transduction, cells were lysed by addition of TRIZOL reagent (Invitrogen) and RNA extracted according to the

manufacturer's instructions. After DNase treatment (Invitrogen), RNA was reverse transcribed into cDNA using an oligo d(T) primer and the Omniscript RT kit (Qiagen).

To quantify target gene expression, following primers were used:

AKTIP Forward 5'-TCCACGCTTGGTGTTCGAT-3'

AKTIP Reverse 5'-TCACCTGAGGTGGGATCAACT-3'

GAPDH Forward 5'-TGGGCTACACTGAGCACCAG-3'

GAPDH Reverse 5'-GGGTGTCGCTGTTGAAGTCA-3'

Western blotting

Whole protein extracts were obtained by treating cell with lysis buffer (20 mM HEPES pH 7.5, 150 mM NaCl, 5 mM MgCl2, 0.5 mM EGTA, 0.25% NP-40, 1 mM DTT, 0.5 mMPMSF, 0.5 mMNa3VO4 and protease inhibitor cocktail, Roche). Samples were loaded onto pre-cast 4–12% gradient acrylamide gels (NuPage, Invitrogen). After electro-blotting, filters were incubated O/N at 4°C with rabbit anti-AKTIP (1:400, Sigma HPA046300), anti-actin-HRP conjugated (1:3500, Santa Cruz 1615) for 1h. Filters were then incubated with appropriate HRP conjugated

secondary antibodies (Santa Cruz; diluted according to the manufacturer's instructions), which were detected using the enhanced chemiluminescence system (ECL Plus, Amersham). Bands were imaged with the ChemiDoc MP imager (Bio-Rad) and band intensities were quantified using the IMAGE LAB software (Bio-Rad).

Yeast Two-Hybrid Assays

Yeast Y190 cells were co-transformed with plasmids encoding the indicated proteins fused to the VP16 activation domain (pHB18) or the Gal4 DNA-binding domain (pGBKT7). Co-transformants were selected on SD-Leu-Trp agar for 3 days at 30°C, harvested, and LacZ activity was measured using a liquid β-galactosidase assay employing chlorophenolred-ß-D-galactopyranoside (Roche) as substrate.

GST pull down

VPS28 was cloned as a GST-fusion into pCAGGS/GST-EcoRI-NotI-XhoI. 293T cells were co-trasfected with 1μg per well of 6-

well plate of either pCAGGS/GST or pCAGGS/GSTVps28 or with 1μg per well of 6-well plate of AKTIP-HA (pCR3.1) for 48hours. Cells were then harvested and lysed in 1 ml of 50 mM Tris·HCl, pH 7.4, 150 mM NaCl,5 mM EDTA, 5% glycerol, 1% Triton X-100, and a protease inhibitor mixture (complete mini-EDTA-free, Roche Applied Science). Clarified lysates were incubated with glutathione-Sepharose beads (Amersham Biosciences) for 3 h at 4 °C and washed three times withwash buffer (50 mM Tris·HCl, pH 7.4, 150 mM NaCl, 5 mM EDTA, 5% glycerol, 0.1% Triton X-100). Bead-bound proteins were resolved by SDS-PAGE and examined by western blotting.

Immunofluorescence and Live-Cell Microscopy

For immunostaining, cells were fixed with 3.7% formaldehyde for 10 min at 4°C and permeabilized with 0.25% Triton X-100 in PBS for 5 min. Cells were then treated with PBS 3% BSA for 30min, then stained with primary antibodies in PBS 1% BSA for 1hour at RT. The following primary antibodies were used: anti-AKTIP (WH0064400M2 (clone 2A11), Sigma), anti-α–tubulin [YL1/2]

Rat monoclonal (Abcam, ab6160), anti-CHMP4B (Proteintech, 13683-1-AP), anti-IST1 (Proteintech), anti-CHMP2A (Proteintech, 10477-1-AP), anti-Lamin B1 (SantaCruz), anti-Lamin A/C (SantaCruz), anti-TRP (abcam ab84516), anti-FLAG (Sigma F1804). Alexa488, Alexa568 or Alexa647 conjugated secondary antibodies were applied in PBS for 45 min at RT. Nuclei were visualized using DAPI (4,6 diamidino-2-phenylindole) and coverslips were mounted in Vectashield H-1000.

Slides were imaged using Zeiss AxioImager Z1 (EBL) equipped with a Axiocam 506 color.

Confocal laser scanning microscopy was performed with Corrsight confocal scanning microscope. Greyscale images were pseudocoloured and combined in Adobe Photoshop CC to create merged images.

Live-cell video microscopy was carried out on Corrsight confocal scanning microscope. siRNA-transfected HeLa cells stably expressing mCherry-tubulin were cultured in a 37°C microscope chamber with 5% CO2 and observed by phase contrast. Images

were acquired every 5 min. Images were then analyzed with ImageJ (National Institutesof Health, Bethesda, MD).

3D-SIM super-resolution microscopy and image analysis

Cells were grown on microscopy cover glasses in 6-well plates, fixed in 3.7% formaldehyde in PBS for 10 min at room temperature and incubated in 50 mM NH4Cl/PBS (5 min). Primary and secondary antibodies were applied in PBS-BSA 1% for 1 hr at room temperature and washed in PBS.

Acquisition was performed using a DeltaVision OMX v4 Blaze microscope (GE Healthcare, Singapore), with the BGR-FR filter drawer for acquisition of 3D-SIM images. Olympus Plan Apochromat 100×/1.4 PSF oil immersion objective lens was used, with liquid-cooled Photometrics Evolve EM-CCD cameras for each channel. 15 images per section per channel were acquired with a z- spacing of 0.125 μm (Schermelleh et al., 2010). Structured illumination reconstruction and wavelength alignment

was completed using the SoftWorX (GE Healthcare). 3D volume reconstructions were done in Imaris (Bitplane).

Statistics

Data and statistical analyses were performed using Excel and Graphpad Prism software. Results are shown as mean ± SEM. Data were analyzed using unpaired two-tailed Student's t-test. p-values below 0.05 were considered significant.

Image quantifications

Structured illumination reconstruction and wavelength alignment was completed using the SoftWorX (GE Healthcare). 3D volume reconstructions and movies generation were done in Imaris (Bitplane). Image analysis and quantification was performed using Fiji (Schindelin et al., 2012), Excel (Microsoft) and Prism (Graphpad) software. Fluorescence intensity values represent the average fluorescence intensity measured from a 2.7µm wide band along the axis of the tubulin bundle.

REFERENCES

Aaronson RP., Blobel G., (1975). Isolation of nuclear pore complexes in association with a lamina. Proc Natl Acad Sci USA., 72(3):1007-11.

Adell MA., Teis D., (2011). Assembly and disassembly of the ESCRT-III membrane scission complex. FEBS Lett., 585 pp. 3191-3196

Agromayor M., Carlton JG., Phelan JP., Matthews DR., Carlin LM., Ameer-Beg S., Bowers K., and Martin-Serrano J., (2009). Essential role of hIST1 in cytokinesis. Mol. Biol. Cell 20, 1374–1387.

Alam SL., Sun J., Payne M., Welch BD., Blake BK., Davis DR., Meyer HH., Emr SD., and Sundquist WI., (2004). Ubiquitin interactions of NZF zinc fingers. EMBO J. 23, 1411–1421.

Andres V. and Gonzalez JM., (2009). Role of A-type lamins in signaling, transcription, and chromatin organization. J. Cell Biol. 187, 945-957.

Asao H., Sasaki Y., Arita T., Tanaka N., Endo K., Kasai H., Takeshita T., Endo Y., Fujita T., and Sugamura K., (1997). Hrs is associated with STAM, a signal-transducing adaptor molecule. Its suppressive effect on cytokineinduced cell growth. J. Biol. Chem. 272, 32785–32791.

Azmi I., Davies B., Dimaano C., Payne J., Eckert D., Babst M., and Katzmann DJ., (2006). Recycling of ESCRTs by the AAA-ATPase Vps4 is regulated by a conserved VSL region in Vta1. J. Cell Biol. 172, 705–717.

Babst M., Katzmann DJ., Snyder WB., Wendland B., and Emr SD. (2002). Endosome-associated complex, ESCRT-II, recruits transport machinery for protein sorting at the multivesicular body. Dev. Cell 3, 283–289.

Bache KG., Raiborg C., Mehlum A., and Stenmark H., (2003). STAM and Hrs are subunits of a multivalent ubiquitin-binding complex on early endosomes. J. Biol. Chem. 278, 12513–12521.

Bache KG., Slagsvold T., Cabezas A., Rosendal KR., Raiborg C., and Stenmark H., (2004). The growth-regulatory protein HCRP1/hVps37A is a subunit of mammalian ESCRT-I and mediates receptor down-regulation. Mol. Biol. Cell 15, 4337–4346.

Bajorek M., Schubert HL., McCullough J., Langelier C., Eckert DM., Stubblefield WM., Uter NT., Myszka DG., Hill CP., and Sundquist WI., (2009). Structural basis for ESCRT-III protein autoinhibition. Nat. Struct. Mol. Biol. 16, 754–762.

Barlow AL., Macleod A., Noppen S., Sanderson J. and Guérin CJ., (2010). Colocalization analysis in fluorescence micrographs: verification of a more accurate calculation of pearson's correlation coefficient. Microsc. Microanal. 16, 710–724.

Bishop N., and Woodman P., (2001). TSG101/mammalian VPS23 and mammalian VPS28 interact directly and are recruited to VPS4-induced endosomes. J. Biol. Chem. 276, 11735–11742.

Burla R., Carcuro M., La Torre M., Fratini F., Crescenzi M., D'Apice MR,. Spitalieri P., Raffa GD., Astrologo L., Lattanzi G.,

Cundari E., Raimondo D., Biroccio A., Gatti M., Saggio I., (2016). The telomeric protein AKTIP interacts with A- and B-type lamins and is involved in regulation of cellular senescence. Open Biol., 6(8):1-11.

Burla R., Carcuro M., Raffa GD., Galati A., Raimondo D., Rizzo A., La Torre M., Micheli E., Ciapponi L, Cenci G., Cundari E., Musio A., Biroccio A., Cacchione S., Gatti M., Saggio I., (2015). AKTIP/Ft1, a New Shelterin-Interacting Factor Required for Telomere Maintenance. Plos Genet., 11: e1005167.

Butin-Israeli V., Adam SA., Goldman AE., Goldman RD., (2012). Nuclear lamin functions and disease. Trends Genet. 28, 464–471.

Canman JC., Hoffman DB., Salmon ED., (2000). The role of pre- and post-anaphase microtubules in the cytokinesis phase of the cell cycle. Curr Biol 10: 611–614.

Capell BC., and Collins FS., (2006). Human laminopathies: nuclei gone genetically awry. Nature Reviews Genetics volume 7, pages 940–952.

Carlton JG., (2010). The ESCRT machinery: a cellular apparatus for sorting and scission. Biochemical Society Transactions, 38 (6) 1397-1412.

Carlton JG., Agromayor M., Martin-Serrano J., (2008). Differential requirements for Alix and ESCRT-III in cytokinesis and HIV-1 release. Proc Natl Acad Sci U S A.; 105(30):10541–10546.

Carlton JG., Martin-Serrano J., (2007). Parallels Between Cytokinesis and Retroviral Budding: A Role for the ESCRT Machinery. Science Vol. 316, Issue 5833, pp. 1908-1912.

Cenci G., Ciapponi L., Marzullo M., Raffa G., Morciano P., Raimondo D., Burla R., Saggio I., Gatti M., (2015). The analysis of pendolino (peo) mutants reveals differences in the fusigenic potential among Drosophila telomeres. PLoS Genetics, 11(6).

Christ L., Wenzel EM., Liestøl K., Raiborg C., Campsteijn C., Stenmark H., (2016). ALIX and ESCRT-I/II function as parallel ESCRT-III recruiters in cytokinetic abscission. J Cell Biol 2016, 212:499-513.

Chu T., Sun J., Saksena S., and Emr S.D. (2006). New component of ESCRT-I regulates endosomal sorting complex assembly. J. Cell Biol. 175, 815–823.

Connell JW., Lindon C., Luzio JP., and Reid E., (2009). Spastin couples microtubule severing to membrane traffic in completion of cytokinesis and secretion. Traffic 10, 42–56.

Corrigan DP., Kuszczak D., Rusinol AE., Thewke DP., Hrycyna CA., Michaelis S., and Sinensky MS., (2005). Prelamin A endoproteolytic processing in vitro by recombinant Zmpste24. Biochem. J. 387, 129-138.

Curtiss M., Jones C., and Babst M. (2007). Efficient cargo sorting by ESCRT-I and the subsequent release of ESCRT-I from multivesicular bodies requires the subunit Mvb12. Mol. Biol. Cell 18, 636–645.

D'Avino PP., Capalbo L., (2016). Regulation of midbody formation and function by mitotic kinases. Semin Cell Dev Biol., 53():57-63.

Dechat T., Gesson K. and Foisner R., (2010). Lamina-independent lamins in the nuclear interior serve important functions. Cold Spring Harb. Symp. Quant. Biol. 75, 533-543.

Dechat T., Pfleghaar K., Sengupta K., Shimi T., Shumaker D., Solimando L., Goldman R., (2008). Nuclear lamins: major factors in the structural organization and function of the nucleus and chromatin. Genes Dev. 22, 832–853.

Denais CM., Gilbert RM., Isermann P., McGregor AL., Lindert Te M., Weigelin B., Davidson PM., Friedl P., Wolf K., Lammerding J., (2016). Nuclear envelope rupture and repair during cancer cell migration. Science, 352:353-358.

Dittmer TA., Misteli T., (2011). The lamin protein family. Genome Biol., 12(5):222.

Doubaj Y., De Sandre-Giovannoli A., Vera EV., Navarro CL., Elalaoui SC., Tajir M., Lévy N., Sefiani A., (2012). An inherited LMNA gene mutation in atypical Progeria syndrome. Am J Med Genet A., 158A(11):2881-7.

Elia N., Sougrat R., Spurlin T.A., Hurley J.H., and Lippincott-Schwartz J., (2011). Dynamics of endosomal sorting complex required for transport (ESCRT) machinery during cytokinesis and its role in abscission. Proc. Natl. Acad. Sci. USA 108, 4846–4851.

Eriksson M., Brown WT., Gordon LB., Glynn MW., Singer J., Scott L., Erdos MR., Robbins CM., Moses TY., Berglund P., Dutra A., Pak E., Durkin S., Csoka AB., Boehnke M., Glover TW., Collins FS., (2003). Recurrent de novo point mutations in lamin A cause Hutchinson-Gilford progeria syndrome. Nature 423(6937):293-8.

Fawcett DW., (1966). On the occurrence of a fibrous lamina on the inner aspect of the nuclear envelope in certain cells of vertebrates. Am J Anat., 119(1):129–45.

Gatta AT., Carlton JG., (2019). The ESCRT-machinery: closing holes and expanding roles. Curr Opin Cell Biol, 59, pp. 121-132.

Gill DJ., Teo H., Sun J., Perisic O., Veprintsev DB., Emr SD., Williams RL., (2007). Structural insight into the ESCRT-I/-II link and its role in MVB trafficking. Embo J., 26:600–612.

Goldman RD., Shumaker DK., Erdos MR., Eriksson M., Goldman AE., Gordon LB., Gruenbaum Y., Khuon S., Mendez M., Varga R. et al., (2004). Accumulation of mutant lamin A causes progressive changes in nuclear architecture in Hutchinson-Gilford progeria syndrome. Proc. Natl. Acad. Sci. USA 101, 8963-8968.

Goldberg MW., Huttenlauch I., Hutchison CJ., Stick R., (2008). Filaments made from A- and B-type lamins differ in structure and organization. J Cell Sci., 121(Pt 2):215-25.

Goliand I., Adar-Levor S., Segal I., Nachmias D., Dadosh T., Kozlov MM., Elia N., (2018). Resolving ESCRT-III Spirals at the Intercellular Bridge of Dividing Cells Using 3D STORM. Cell Rep, 24 pp. 1756-1764.

Goliand I., Nachmias D., Gershony O., Elia N., (2014). Inhibition of ESCRTII-CHMP6 interactions impedes cytokinetic abscission and leads to cell death. Mol Biol Cell, 25:3740-3748.

Gordon LB., Rothman FG., Lopez-Otın C., Misteli T., (2014). Progeria: a paradigm for translational medicine. Cell, 156:400-407.

Gromley A., Yeaman C., Rosa J., Redick S., Chen CT., Mirabelle S., Guha M., Sillibourne J., Doxsey SJ., (2005). Centriolin anchoring of exocyst and SNARE complexes at the midbody is required for secretory-vesicle-mediated abscission. Cell, 123 pp. 75-87.

Gruenbaum Y., Margalit A., Goldman RD., Shumaker DK., and Wilson KL., (2005). Nature Reviews Molecular Cell Biology volume 6, pages21–31

Guizetti J., Schermelleh L., Mantler J., Maar S., Poser I., Leonhardt H., Muller-Reichert T., and Gerlich DW., (2011). Cortical constriction during abscission involves helices of ESCRT-III-dependent filaments. Science 331, 1616–1620.

Herrmann H., and Foisner R., (2003). Intermediate filaments: novel assembly models and exciting new functions for nuclear lamins. Cell. Mol. Life Sci. 60, 1607-1612.

Hu CK., Coughlin M., Field CM., Mitchison TJ., (2011). KIF4 regulates midzone length during cytokinesis. Curr Biol., 21(10):815-24.

Hurley JH., (2015). ESCRTs are everywhere. EMBO J (2015)34:2398-2407.

Jimenez AJ., Maiuri P., Lafaurie-Janvore J., Divoux S., Piel M., Perez F., (2014). ESCRT machinery is required for plasma membrane repair. Science, 343:1247136.

Karasmanis EP., Hwang D., Nakos K., Bowen JR., Angelis D., Spiliotis ET., (2019). A septin double ring controls the spatiotemporal organization of the ESCRT machinery in cytokinetic abscission. Curr Biol., 29(13):2174–2182.e7.

Katzmann DJ., Babst M., and Emr SD., (2001). Ubiquitin-dependent sorting into the multivesicular body pathway requires

the function of a conserved endosomal protein sorting complex, ESCRT-I. Cell 106, 145–155.

Katzmann DJ., Stefan CJ., Babst M., and Emr SD., (2003). Vps27 recruits ESCRT machinery to endosomes during MVB sorting. J. Cell Biol. 162, 413–423.

Kostelansky MS., Sun J., Lee S., Kim J., Ghirlando R., Hierro A., Emr SD., and Hurley JH., (2006). Structural and functional organization of the ESCRT-I trafficking complex. Cell 125, 113–126.

Kubben N., Zhang W., Wang L., Voss TC., Yang J., Qu J., Liu GH., Misteli T., (2016). Repression of the Antioxidant NRF2 Pathway in Premature Aging. Cell, 165(6):1361-1374.

La Torre M., Merigliano C., Burla R., Mottini C., Zanetti G., Del Giudice S., Carcuro M., Virdia I., Bucciarelli E., Manni I., Vinciguerra GR., Piaggio G., Riminucci M., Cumano A., Bartolazzi A., Vernì F., Soddu S., Gatti M., Saggio I., (2018). Mice

with reduced expression of the telomere-associated protein Ft1 develop p53-sensitive progeroid traits. Aging Cell., e12730.

Langelier C., von Schwedler UK., Fisher RD., De Domenico I., White PL., Hill CP., Kaplan J., Ward D., and Sundquist WI., (2006). Human ESCRT-II complex and its role in human immunodeficiency virus type 1 release. J. Virol. 80, 9465–9480.

Lattanzi G., Benedetti S., D'Apice MR., Maggi L., Carboni N., Scarano E., Politano L., (2016). Emerging perspectives on laminopathies. Cell Health Cytoskelet., 8:25–35.

Lee HH., Elia N., Ghirlando R., Lippincott-Schwartz J., and Hurley J.H., (2008). Midbody targeting of the ESCRT machinery by a noncanonical coiled coil in CEP55. Science 322, 576–580.

Li M., Rong Y., Chuang YS., Peng D., Emr SD., (2015)., Ubiquitin-dependent lysosomal membrane protein sorting and degradation. Cell, 57(3): p. 467-78.

Lin F., Worman HJ., (1993). Structural organization of the human gene encoding nuclear lamin A and nuclear lamin C. J Biol Chem., 268:16321–6.

Lutz RJ., Trujillo MA., Denham KS., Wenger L. and Sinensky M., (1992). Nucleoplasmic localization of prelamin A: implications for prenylation-dependent lamin A assembly into the nuclear lamina. Proc. Natl. Acad. Sci. USA 89, 3000-3004.

Mao Y., Nickitenko A., Duan X., Lloyd TE., Wu MN., Bellen H., and Quiocho FA., (2000). Crystal structure of the VHS and FYVE tandem domains of Hrs, a protein involved in membrane trafficking and signal transduction. Cell 100, 447–456.

Matsuo M., Shimodaira T., Kasama T., Hata Y., Echigo A., Okabe M., et al., (2013). Katanin p60 contributes to microtubule instability around the midbody andfacilitates cytokinesis in rat cell. PLoS One 8, e80392.

McCullough J., Frost A., and Sundquist WI., (2018). Structures, functions, and dynamics of ESCRT-III/Vps4 membrane

remodeling and fission complexes. Annu. Rev. Cell Dev. Biol. 2018.34:85-109.

Mendez-Lopez I., Worman HJ., (2012). Inner nuclear membrane proteins: impact on human disease. Chromosoma, 121(2):153-67.

Morita E., Sandrin V., Chung HY., Morham SG., Gygi SP., Rodesch CK., Sundquist WI., (2007). Human ESCRT and ALIX proteins interact with proteins of the midbody and function in cytokinesis. EMBO J, 26:4215-4227.

Muchir A., van Engelen BG., Lammens M., Mislow JM., McNally E., Schwartz K., Bonne G., (2203). Nuclear envelope alterations in fibroblasts from LGMD1B patients carrying nonsense Y259X heterozygous or homozygous mutation in lamin A/C gene. Exp Cell Res., 291(2):352-62.

Muzio1 T., Pineda-Molina E., Ravelli RB., Zamborlini A., Usami Y., Gottlinger H., and Weissenhorn W., (2006). Structural basis for budding by the ESCRT-III factor CHMP3. Dev. Cell 10, 821–830.

Olmos Y., Hodgson L., Mantell J., Verkade P., Carlton JG., (2015). ESCRT-III controls nuclear envelope reformation. Nature, 522(7555):236-9.

Olmos Y., Perdrix-Rosell A., Carlton JG., (2016). Membrane binding by CHMP7 coordinates ESCRT-III-dependent nuclear envelope reformation. Curr Biol, 26:2635-2641.

Ostlund C., Bonne G., Schwartz K., Worman HJ., (2001). Properties of lamin A mutants found in Emery-Dreifuss muscular dystrophy, cardiomyopathy and Dunnigan-type partial lipodystrophy. J Cell Sci., 114(Pt 24):4435-45.

Patrizi G., Poger M., (1967). The ultrastructure of the nuclear periphery. The zonula nucleum limitans. J Ultrastruct Res., 17(1):127-36.

Pegoraro G., Kubben N., Wickert U., Gohler H., Hoffmann K., Misteli T., (2009). Ageing-related chromatin defects through loss of the NURD complex. Nat. Cell Biol. 11, 1261–1267.

Pohl C., Jentsch S., Midbody ring disposal by autophagy is a post-abscissionevent of cytokinesis, Nat. Cell Biol. 11 (2009) 65–70.

Prokocimer M., Davidovich M., Nissim-Rafinia M., Wiesel-Motiuk N., Bar DZ., Barkan R., Meshorer E. and Gruenbaum Y., (2009). Nuclear lamins: key regulators of nuclear structure and activities. J. Cell. Mol. Med. 13, 1059-1085.

Raab M., Gentili M., de Belly H., Thiam HR., Vargas P., Jimenez AJ., Lautenschlaeger F., Voituriez R., Lennon-Dumenil AM., Manel N., et al., (2016). ESCRT III repairs nuclear envelope ruptures during cell migration to limit DNA damage and cell death. Science, 352:359-362.

Raiborg C., Bremnes B., Mehlum A., Gillooly DJ., D'Arrigo A., Stang E., and Stenmark H. (2001)., FYVE and coiled-coil domains determine the specific localisation of Hrs to early endosomes. J. Cell Sci. 114, 2255–2263.

Ren X., Kloer DP., Kim YC., Ghirlando R., Saidi LF., Hummer G., and Hurley JH., (2009). Hybrid structural model of the complete human ESCRT-0 complex. Structure 17, 406–416.

Robijns J., Molenberghs F., Sieprath T., Corne TDJ., Verschuuren M., De Vos WH., (2016). In silico synchronization reveals regulators of nuclear ruptures in lamin A/C deficient model cells. Sci Rep, 6:30325.

Rusinol AE., Sinensky MS., (2006). Farnesylated lamins, progeroid syndromes and farnesyl transferase inhibitors. J Cell Sci., 119(Pt 16):3265-72.

Scaffidi P., Misteli T., (2006). Lamin A-dependent nuclear defects in human aging. Science, 312(5776):1059-63.

Scheffer LL., Sreetama SC., Sharma N., Medikayala S., Brown KJ., Defour A., Jaiswal JK., (2014). Mechanism of Ca2+-triggered ESCRT assembly and regulation of cell membrane repair. Nat Commun, 5:5646.

Schermelleh L., Heintzmann R., Leonhardt H., (2010). A guide to super-resolution fluorescence microscopy. J Cell Biol.; 190(2):165–175.

Schindelin J., Arganda-Carreras I., Frise E., Kaynig V., Longair M., Pietzsch T., Preibisch S., Rueden C., Saalfeld S., Schmid B., Tinevez JY., White DJ., Hartenstein V., Eliceiri K., Tomancak P., Cardona A., (2012). Fiji: an open-source platform for biological-image analysis. Nat Methods 9, 676-682.

Schmidt O., Teis D., (2012). The ESCRT machinery. Curr. Biol., 22 (Feb 4) (2012), pp. R116-20

Schoneberg J., Lee IH, Iwasa JH., Hurley JH., (2017). Reverse-topology membrane scission by the ESCRT proteins. Nature Reviews Molecular Cell Biology volume 18, pages 5–17.

Straight AF., Field CM., (2000). Microtubules, membranes and cytokinesis. Curr Biol 10: R760–R770.

Shimi T., Pfleghaar K., Kojima S., Pack CG., Solovei I., Goldman AE., Adam SA., Shumaker DK., Kinjo M., Cremer T., Goldman

RD., (2008). The A- and B-type nuclear lamin networks: microdomains involved in chromatin organization and transcription. Genes Dev., 22(24):3409-21.

Stuurman N., Heins S., and Aebi U., (1998). Nuclear lamins: their structure, assembly, and interactions. J. Struct. Biol. 122, 42-66.

Teo H., Perisic O., Gonzalez B., and Williams RL., (2004). ESCRT-II, an endosome-associated complex required for protein sorting: crystal structure and interactions with ESCRT-III and membranes. Dev. Cell 7, 559–569.

Vietri M., Schink KO., Campsteijn C., Wegner CS., Schultz SW., Christ L., Thoresen SB., Brech A., Raiborg C., Stenmark H., (2015). Spastin and ESCRT-III coordinate mitotic spindle disassembly and nuclear envelope sealing. Nature, 522:231-235.

Vigouroux C., Auclair M., Dubosclard E., Pouchelet M., Capeau J., Courvalin JC., Buendia B., (2001). Nuclear envelope disorganization in fibroblasts from lipodystrophic patients with

heterozygous R482Q/W mutations in the lamin A/C gene. Cell Sci., 114(Pt 24):4459-68.

Vorburger K., Lehner CF., Kitten GT., Eppenberger HM., Nigg EA., (1989). A second higher vertebrate B-type lamin. cDNA sequence determination and in vitro processing of chicken lamin B2. J Mol Biol, 208, pp. 405-415.

Wheatley SP., Wang Y., (1996). Midzone microtubule bundles are continuously required for cytokinesis in cultured epithelial cells. J Cell Biol 135: 981–989.

Wilson KL. and Berk JM., (2010). The nuclear envelope at a glance. J. Cell Sci. 123, 1973-1978.

Wilson KL. and Foisner R., (2010). Lamin-binding Proteins. Cold Spring Harb. Perspect. Biol. 2, a000554.

Winter-Vann AM., and Casey PJ., (2005). Post-prenylation-processing enzymes as new targets in oncogenesis. Nat. Rev. Cancer 5, 405-412.

Wollert T., Wunder C., Lippincott-Schwartz J., Hurley JH., (2009). Membrane scission by the ESCRT-III complex. Nature 458 pp. 172-177.

Xu L., Sowa ME., Chen J., Li X., Gygi SP., Harper JW., (2008). An FTS/Hook/p107(FHIP) complex interacts with and promotes endosomal clustering by the homotypic vacuolar protein sorting complex. Mol Biol Cell., 19(12): p. 5059-71.

Yang LW., Radebaugh JF., Rubin P., Sensenbrenner JA., Fiorelliu G., McKusick VA., (1971). New syndrome manifested by mandibular hypoplasia, acroosteolysis, stiff joints and cutaneous atrophy (mandibuloacral dysplasia) in two unrelated boys. Birth Defects Org Artic Ser., 7:291–297.

Ye Y., Rape M., (2009). Building ubiquitin chains: E2 enzymes at work. Nat Rev Mol Cell Biol, 10(11):755–64.

Yu Z., Gonciarz MD., Sundquist WI., Hill CP., and Jensen GJ., (2008). Cryo-EM structure of dodecameric Vps4p and its 2:1 complex with Vta1p. J. Mol. Biol. 377, 364–377.

Zhang FL., and Casey PJ., (1996). Protein prenylation: molecular mechanisms and functional consequences. Annu. Rev. Biochem. 65, 241-269.

Zhang J., Lian Q., Zhu G., Zhou F., Sui L., Tan C., Mutalif RA., Navasankari R., Zhang Y., Tse HF., Stewart CL., Colman A., (2011). A human iPSC model of Hutchinson Gilford Progeria reveals vascular smooth muscle and mesenchymal stem cell defects. Cell Stem Cell., 8(1):31-45.

LIST OF PUBBLICATION

Romina Burla, Mattia la Torre, Giorgia Zanetti, Alex Bastianelli, Chiara Merigliano, Simona Del Giudice, Alessandro Vercelli, Ferdinando Di Cunto, Marina Boido, Fiammetta Vernì and Isabella Saggio. p53- sensitive epileptic behavior and inflammation in Ft1 hypomorphic mice. Frontiers in Genetics, November 2018

Mattia la Torre, Chiara Merigliano, Romina Burla, Carla Mottini, Giorgia Zanetti, Simona Del Giudice, Mariateresa Carcuro, Ilaria Virdia, Elisabetta Bucciarelli, Isabella Manni, Gianluca Rampioni Vinciguerra, Giulia Piaggio, Mara Riminucci, Ana Cumano, Armando Bartolazzi, Fiammetta Verni, Silvia Soddu, Maurizio Gatti, Isabella Saggio. Mice with reduced expression of the telomere-associated protein Ft1 develop p53-sensitive progeroid traits. Aging Cell, April 2018.

Domenico Raimondo; Cristina Remoli; Letizia Astrologo; Romina Burla; Mattia La Torre; Fiammetta Verni'; Enrico Tagliafico; Alessandro Corsi; Simona Del Giudice; Agnese Persichetti; Giuseppe Giannicola; Pamela Robey; Mara Riminucci; Isabella

Saggio. Changes in gene expression in human skeletal stem cells transduced with constitutively active Gsα correlates with hallmark histopathological changes seen in fibrous dysplastic bone. plos one submitted 2019.